Weathering intensities in tropical soils evaluated by machine learning, clusterization and geophysical sensors

Danilo César de Mello[1], Tiago Osório Ferreira[2], Gustavo Vieira Veloso[1], Marcos Guedes de Lana[1],
Fellipe Alcantara de Oliveira Mello[2], Luis Augusto Di Loreto Di Raimo[2], Diego Ribeiro Oquendo

5 Cabrero[3], José João Lelis Leal de Souza[1], Elpídio Inácio Fernandes-Filho[1], Márcio Rocha Francelino[1],
Carlos Ernesto Gonçalves Reynaud Schaefer[1], José A. M. Demattê[2]

[1]Department of Soil Science, Federal University of Viçosa, Viçosa, postal code 36.570-000, Brazil, e-mails:
daniloc.demello@gmail.com; gustavo.v.veloso@gmail.com; marcosguedeslana@gmail.com; jjlelis@ufv.br;
marcio.francelino@ufv.br; elpidio@ufv.br; carlos.schaefer@ufv.br

10 [2] Department of Soil Science, "Luiz de Queiroz" College of Agriculture, University of São Paulo, Piracicaba, postal code
13418-900, Brazil, e-mails; toferreira@usp.br; jamdemat@usp.br; fellipeamello@usp.br; luis.diloreto@hotmail.com;

[3] Geography Department of Federal University of Mato Grosso do Sul, Três Lagoas, postal code 79610-100, Brazil: e-mail:
diego.cabrero@gmail.com

Correspondence to: José A. M. Demattê (jamdemat@usp.br)

15 **Abstract:** Weathering is widely used for pedogenesis and soil fertility studies, once it affects several soil attributes.
Understanding the intensities of weathering can provide answers for environmental issues, soil and geosciences studies.
Recently, there are available geotechnologies (such as geophysics and machine learning algorithms) that can be applied in
soil science to provide pedosphere information. In this research, we performed a method to evaluate weathering intensity in a
heterogeneous tropical area by proximal remote sensing data acquired by geophysical and satellite images respectively. The

20 area is located in southwest Brazil, with 184 h and we sampled 79 sites (all with soil analysis) using toposequence
knowledge. Afterwards, the principal component analysis and the ideal number of clusters was determined. Then, we
determine and used the ideal number of clusters, weathering index, as input data in four modelling (prediction and
spatialization) algorithms to infer different weathering intensities in soils formed from the same soil parent material. The
results showed that the best model performance was for the random forest reaching 3 clusters as the ideal number. The

25 surface pixel reflectance acquired from a Synthetic Soil Image, the terrain surface convexity and digital elevation model
were the covariates that most contributed to modelling processes. The model' specificity was greater than sensitivity. The
East areas over diabase such as the Nitisol presented greater weathering intensity than the Nitisol over West diabase areas.
The areas over siltite/metamorphosed siltite and Lixisols presented moderate weathering rates. The relief and topographic
position strongly affected the weathering, once they controlled the hydric dynamics. The geophysical variables were related

30 to soil attributes and weathering, which contributed to modelling and clusterization processes. The different weathering rates
are mainly modulated by geomorphic processes that relief, topographic position, and the associated soil types control water
dynamic at the landscape and directly affect the weathering intensities.

1 Introduction

35   Weathering process can be understood as the spontaneous and irreversible responses of rocks, soils and sediments to the prevailing environmental conditions at (or near) the surface as opposed to those where these materials were originated (Carroll, 2012; Santos et al., 2019; White, 2018). The main controlling factors of weathering are: parent material characteristics, climate, relief, organisms and time (Borrelli et al., 2015, 2016; Carroll, 2012). Weathering processes involve simple mechanical disintegration and, chemical-mineralogical changes in rocks and minerals (Borrelli et al., 2014; Regmi et

40   al., 2014; Scarciglia et al., 2016; Apollaro et al., 2019; Santos et al., 2018; Santos et al., 2019).

Weathering mantle can reach varying depths in the pedosphere, depending on the characteristics of the weathered material, on the hydrological conditions and, on the biota activity (Ollier, 1984). On the other hand, the weathering rate refers to the amount of material chemically altered and/or removed per unit of time (Bland & Rolls, 2016). The intensity of weathering, in turn, controls the degree of alteration and, thus, the degree in which primary minerals are transformed into secondary,

45   where an increase in the intensity of weathering results in an increase in the geochemical and geophysical changes of the weathered materials (Wilford, 2012).

Soil weathering studies contribute to the understanding of the spatial variability of different soil types on the landscape (Jenny, 1994; Scarciglia et al., 2005; Yoo et al., 2009), landscape evolution and, geomorphic processes (Migoń, 2013a, 2013b; Turkington et al., 2005), chemical and mineralogical composition of soils and sediments (Jackson and Sherman,

50   1953; Prasetyo et al., 2016; Khelfaoui et al., 2020), concentration of chemical elements for plants (Schuessler et al., 2018; Porder, 2019), potentially toxic elements (Yu et al., 2012; Cabral Pinto et al., 2017), biogeochemical cycles (Torres et al., 2016; Doetterl et al., 2018; Dynarski et al., 2019), land use and management (Kaushal et al., 2017; Linden and Delvaux, 2019; Kim et al., 2020), chemical characteristics of the hydrosphere (Kumar et al., 2019; Tsering et al., 2019), as well as the relationship between pedosphere and other environmental spheres (hydrosphere, biosphere, lithosphere and atmosphere)

55   (Buss et al., 2017).

Many studies demonstrate the relationship between chemical weathering processes and geochemistry of hydrosphere and pedosphere, soil attributes, weathering profiles in specific locations and modeling studies (Gaillardet et al., 1999; Anderson et al., 2004; Lerman et al., 2007; Navarre-Sitchler and Brantley, 2007; Goddéris et al., 2009; Brantley et al., 2011; Maher, 2011). In addition, Terra et al. (2018), using geotechnologies evaluated different rates of weathering and pedogenesis in soil

60   profiles, analyzing changes in soil texture and mineralogical composition by spectroscopic methods.

With the development of new geotechnologies and geophysical techniques, pedologists have studied the relationship between soil attributes, weathering and pedogenesis (Beamish, 2013; McFadden and Scott, 2013; Mello et al., 2020, 2021; Reinhardt and Herrmann, 2019; Schuler et al., 2011). Radiometric, magnetic and electric methods are the main ones used in geophysical surveys and soil science.

65   Gamma-spectrometry is a radiometric method which consists of analyzing the concentration and behavior of uranium (U^{238}), thorium (Th^{232}) and potassium (K^{40}) levels in soils, rocks and sediments (Minty, 1988). In addition to the characteristics of

the parent material, processes that occur in the landscape (e.g., weathering, pedogenesis, erosion and sediment deposition), associated with the pedogeochemical comportment of each radionuclide determine their concentration/distribution in the soil system (Dickson and Scott, 1997; Wilford and Minty, 2006). Studies undertaken by Dickson and Scott, (1997); Wilford and

70 Minty, (2006); Malikova and Strakhovenko, (2017) and Ribeiro et al. (2018) demonstrated the relationship between uranium, thorium and potassium contents with soil attributes, weathering and pedogenetic processes.

Magnetic susceptibility (κ) is a magnetic method. It comprises the degree of magnetism of an given element (how much it can be magnetized) (Rochette et al., 1992). The magnetic susceptibility of the soils is related to their mineralogy, which in turn is related to parent material and pedogeochemistry environment for formation of secondary minerals, generally

75 ferrimagnetic such as magnetite (sand fraction) and maghemite (clay fraction) (Ayoubi et al., 2018) and to a lesser extent in ferrihydrite and hematite (Valaee et al., 2016). Soil magnetic susceptibility can be applied to geological studies (Shenggao, 2000), determination of soil clay/sand content and organic carbon content (Camargo et al., 2014; Jiménez et al., 2017), in soil surveying (Grimley et al., 2004) and in studying of pedogenetic and geomorphological processes (Sarmast et al., 2017; Mello et al., 2020).

80 Apparent electrical conductivity is an electric method. When applied to the soil, it can be defined as the ability of the soil to conduct electric current. The amount of electric current that the soil is able to conduct is mainly in function of the amount and type of solutes in the soil solution. It is usually expressed in millisiemens per meter, with a minimum concentration of 1dS/m equivalent to 10 meq/L (Richards, 1954).

Originally, ECa was used as a measure of soil salinity and, nowadays, it is a technology used to estimate soils properties and

85 their spatial variation (Corwin et al., 2003). The main factors that affect the ECa are: soil salinity, clay content and type, cation exchange capacity, mineralogy, pore size and distribution, temperature, soil moisture (McNeill, 1992; Rhoades et al., 1999; Bai et al., 2013; Cardoso and Dias, 2017). Several studies have demonstrated the relationship between soil ECa and its attributes (Friedman, 2005; Sudduth et al., 2005; Chung et al., 2019; Grubbs et al., 2019; Nocco et al., 2019; Marta et al., 2020). Besides, Son et al. (2010) and Zhu et al. (2016) have used (ECa) to assess the degree of soil weathering and study its

90 pedogenesis, demonstrating the potential of the technique for pedological studies.

However, to our knowledge, there is a scarcity of studies and information that use a combination of geophysical sensors with data from traditional soil analyzes, remote sensing and machine learning algorithms, for detailed studies to assess the intensity of weathering in tropical environments in different types of soils (Goydaragh et al., 2021).

Given above, this research aimed to: *i)* model weathering index using combined data from geophysical sensors, satellite

95 images and morphometry by different machine learning algorithms; *ii)* evaluate the importance of the covariates used in modeling (nested-leave-one-out-cross-validation method) and relate them to pedogeomorphological processes; *iii)* evaluate the quality of weathering index map obtained by remote and geophysical survey data; *iv)* evaluate if geophysical data is more efficient than remote sensing to predict the weathering indexes. Our main hypothesis is that geophysical sensors and satellite can detected how the different intensities of weathering affect, in different manners, the soil attributes and their

100 composition in the same parent material.

We analyzed apparent discrepancies between weathering intensities and some chemical weathering indexes created by geophysical sensors and geochemical indices, chemical evaluation throughout machine learning algorithms. In addition, we focused on a more detailed description of chemical weathering in a complex study area in terms of relief and geology in a tropical environment.

105

2 Material and methods

2.1 Study area and soil samples

The study area has 184 hectares and was located in the municipality of Raffard (22° 59' 39.3" S and 47° 38' 55.7"W), in São

110 Paulo State, Brazil (**Fig 1**). The area was recently cultivated with sugar cane and, it was entirely located on a plowed field. The area is part of the hydrographic basin of the Capivari River, located in the Paulista Peripheric Depression (SE Brazil). The lithology of the area is composed by siltite and metasiltite from the Itararé Formation, diabase from the Serra Geral Formation and, alluvial sediments (**Fig. 2a**).
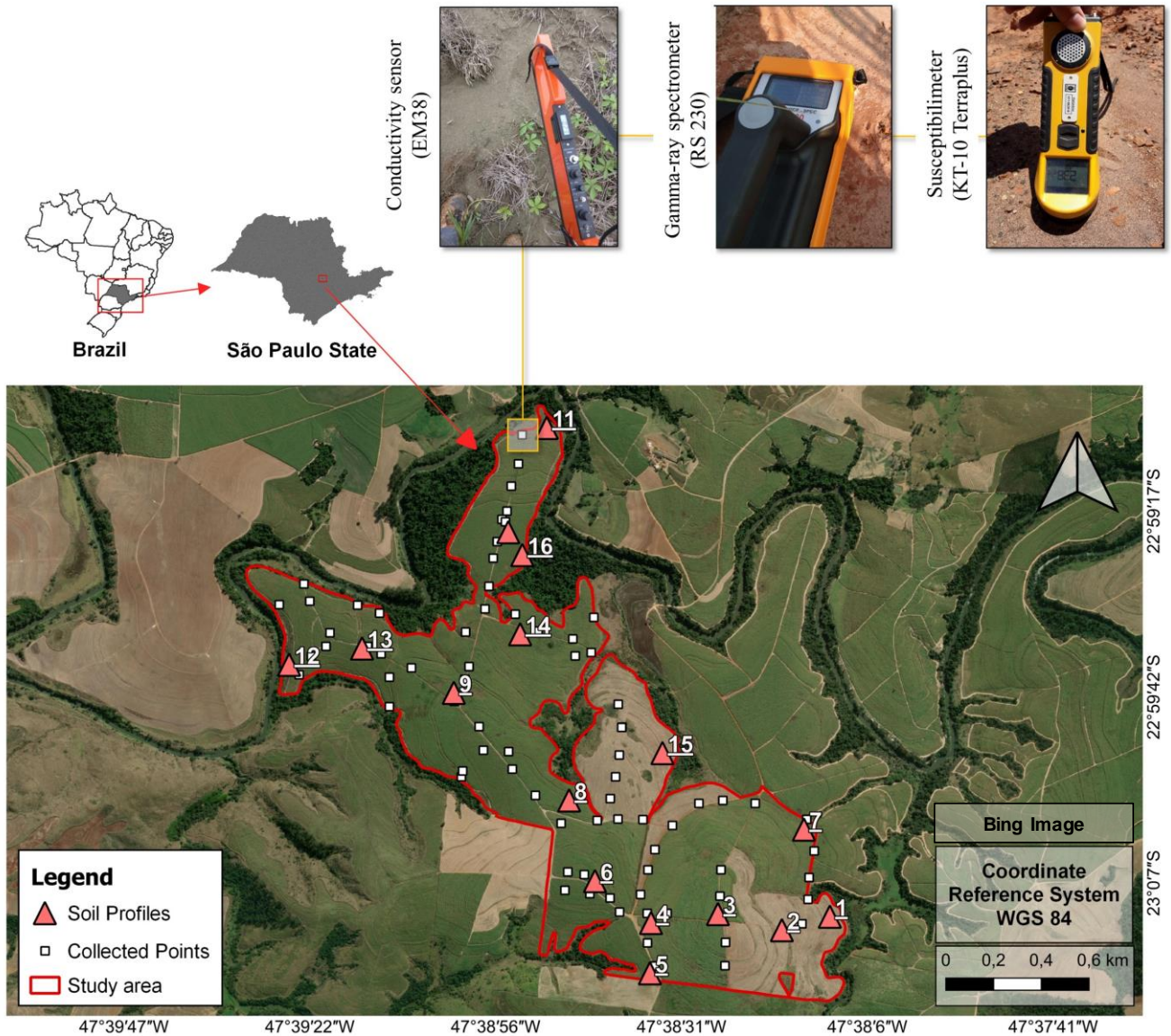
Figure 1. Study area location, site of the collection points and geophysical sensors (Geonics Ground Conductivity Meter - EM 38; Gamma-ray spectrometer - Radiation Solution - RS 230; Susceptibilimeter KT-10 Terraplus). Bing Image from © Microsoft.

The maximum altitude was 567m and the minimum 474m with slope ranging from 0 to 35% (**Fig. 2c and 2d**). The climate of the region was classified according to Köppen system, as subtropical mesothermal (Cwa). The temperatures vary from 18

°C to 22 °C (during winter on July and summer on February, respectively). The mean annual precipitation varies (1100 to 1700 mm) (Alvares et al., 2013).

Soil classification was carried out by an experienced pedologist. For that, 16 representative soil profiles were selected according to the topographic position and variations in relief. Subsequently, all soil profiles were described and classified
125   following IUSS Working Group WRB, (2015). Then, soil samples from all soil horizons were collected for physical-chemical analysis. The main soil types classified in the area were: Cambisols, Phaeozems, Nitisols, Acrisols and Lixisols (IUSS Working Group WRB, 2015) (**Fig. 2b)**. In addition to the soil samples collected in the profiles, soil samples were collected, via augering, for physical-chemical analysis at 79 points distributed according to figure 1. The samples were collected in the 0 - 20cm layer. (**Fig. 1**).

COORDINATE REFERENCE SYSTEM WGS 84
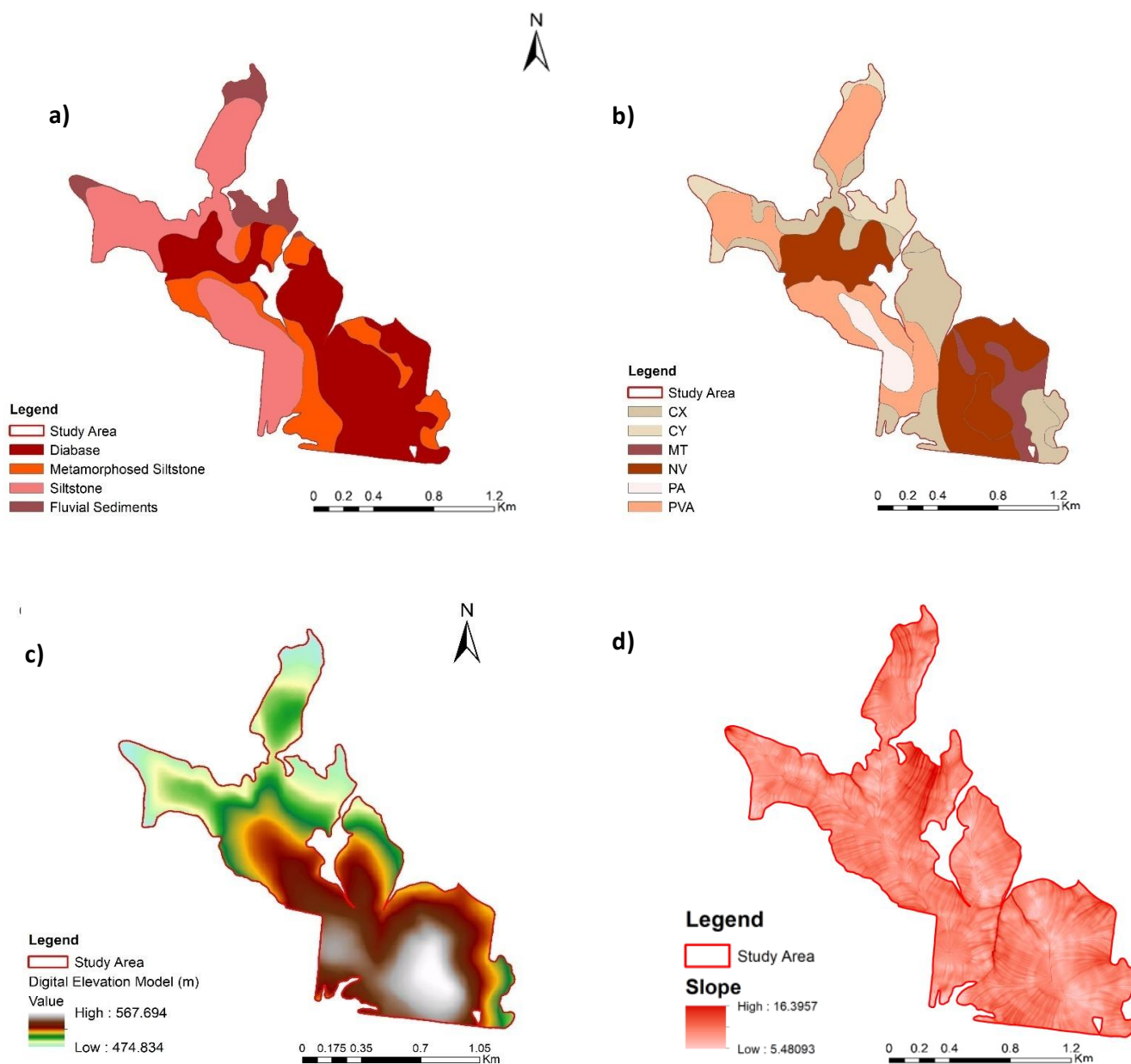
130

Figure 2. a) Geological compartments of landscape. b) Soil classes: CX: Haplic Cambisols, CY: Fluvic Cambisols, MT: Luvic Phaozem, NV: Rhodic Nitisol: PA: Xanthic Acrisol, PVA: Rhodic Lixisol. The geological and Soil classes maps were adapted from Bazaglia Filho et. al. (2012). c) Digital Elevation Model: d) Slope.

2.2. Laboratory analysis

For granulometric analysis all soil samples were air dried, ground and passed through a 2 mm sieve. Then, soil clay, silt and sand content were quantified by densimeter method (Camargo et al., 1986) and textural classification were determined following the EMBRAPA (2011) methodology.

For the extraction of aluminum, magnesium and calcium cations (Ca^{2+}, Mg^{2+} and Al^{3+}, respectively) a solution of 1 mol L^{-1} KCl was used according to EMBRAPA, (2011) method. To extract the potassium cation (K^+), the Melich 1 extractor was used and, the quantification was performed by flame photometry. A solution of concentration 0.5 mol L^{-1} at pH 7 of calcium acetate was used to determine the potential acidity ($H^+ + Al^{3+}$), which was later quantified by titration with 0.025 mol L^{-1} NaOH, following the Shoemaker, Mac lean and Pratt (SMP) method (Quaggio and Raij, 2001).

The pH in water was determined by the electrode method following (EMBRAPA, 2011). The organic carbon content was quantified via oxidation with dichromate (0.167 mol L^{-1} $K_2Cr_2O_7$), following the Walkley–Black method (Walkley and Black, 1934). The total iron content (Fe_2O_3), silicon dioxide (SiO_2) and titanium dioxide (TiO_2) were determined using the EMBRAPA, (2017) methodology. The other soils parameters such as base sum, base saturation, aluminium saturation and cation exchange capacity were calculated using the previous obtained analytical data (EMBRAPA, 2017).

2.3. Weathering rates

To some extend the chemical weathering reactions are controlled by the geochemical behaviour of major elements that composes rocks, soils and sediments (Loughnan, 1962). Thus, the chemical weathering indexes are developed using some of major elements, which quantify the depletion of mobile elements (e.g., those with lower ionic potential) with respect to the immobile elements (Harnois, 1988). Several chemical weathering indices utilize weathering observations of felsic and intermediate igneous rocks under moist, well-drained pedoenvironments, as well as in situ weathering profiles (Duzgoren-Aydin and Aydin, 2003; Harnois, 1988; Nordt and Driese, 2010; Ruxton, 1968).

Weathering indexes traditionally have been calculated using the molecular proportions between major elements expressed as oxides. In this sense, the weathering indexes were calculated following the methodology proposed by Jayawardena and Izawa, (1994), (Eq 1).

$$W1 = \frac{SiO2}{TiO2} X\ 100 \qquad\qquad (1)$$

2.4 Geophysical data collection

2.4.1 Radiometric data (gamma-ray spectrometry)

The values of the uranium (eU), thorium (eTh) and potassium (K[40]) radionuclides were quantified using the portable gamma-ray spectrometer (GM) equipment Radiation Solution RS 230 - Radiation Solution INC - Ontario – Canada (Fig. 1). The sensor is able to detect and quantify the radionuclides at a depth ranging from 30 to 60 cm, depending on the moisture and density of the soil (Wilford et al., 1997; Taylor et al., 2002; Beamish, 2015).

Firstly, the sensor was automatically stabilized. The sensor was placed for two minutes in direct contact with the soil surface, in each sampling point (79), according to figure 1. The measurements were taken in the "assay-mode" of the highest precision for radionuclide quantification. The coordinates of each sampling point were recorded by a GPS connected to the gamma-spectrometer by Bluetooth. The sensor detected eU and eTh in parts per million (ppm) and, K[40] in %. However, the eU and eTh contents were reported in mg kg^{-1}.

2.4.2 Magnetic susceptibility (κ) data

Soil magnetic susceptibility κ values were collected using the sensor model KT10 - Terraplus (**Fig. 1**). This equipment is capable of measuring the κ values at a depth of to 2 cm below the soil surface. Before the measurements, the sensor was properly calibrated following the recommendations of Sales, (2021). The measurements were performed at the 79 collection points (**Fig. 1**), placing the entire sensor base in direct contact with the soil surface. The measurements were performed with the sensor in scanner mode, which provides the values of k more quickly and accurately (with precision 10^{-6} SI units, in m^3 kg^{-1}). We performed three readings around each sampling point to reduce sensor noise and, the averages were used in our analysis.

2.4.3 Apparent electrical conductivity (ECa)

Soil ECa values were acquired using sensor conductivity meter Geonics EM38 (Geonics Ltd., Mississauga, Ontario, Canada) (McNeill, 1986) (**Fig. 1**). For this, first the sensor was properly calibrated according to Heil and Schmidhalter, (2019) recommendations. Measurements were taken with the sensor in a vertical position in direct contact with the soil surface at all 79 collection points (Fig. 1). In this position the EM38 is able to provide soil ECa values down to an effective depth of 1.5 meters. The collections were carried out in the dry season and during the same range of hours of the day to reduce the effects of soil moisture. In addition, all metal objects were kept away to avoid sensor noise. More details on sensor working principles, calibration and factors that affect soil ECa readings can be found in Geonics, (2002); Heil and Schmidhalter, (2019); Hendrickx and Kachanoski, (2002).

It is important to highlight that there were noises for some sensors with extremely abnormal values at 8 reading points. These values were considered outliers and were not used in the analyses. Therefore, the total number of samples used were 71.

2.5 Generation of digital elevation model, slope and maps

195 We obtained contour lines with 5 m contour interval, acquired from plan altimetric maps at 1:10,000 scale, obtained from the Campinas Geographic Institute (IGC). The lines were used to interpolate a digital elevation model (DEM) using the Topo to Raster function in ESRI ArcGIS 10.4. The DEM was exported with 30 m of spatial resolution. We decided to use the calculated DEM from a detailed database to enforce the smallest altitude variations presented in the study area, which are important for discussing the results. Although more accessible altitude information can be used to generate the DEM, such as

200 the Shuttle Radar Topographic Mission (SRTM), the DEM derived from the contour lines expressed the relief in greater detail. Using the DEM data, 32 additional terrain attributes were created (see **Table 1**) using the *R* software (R Core Team, 2015), including the "*Rsaga*" (Brenning, 2008) and "*raster*" (Hijmans and Van Etten, 2016) packages.

Table 1. Terrain attributes generated from the digital elevation model

Terrain attributes	Abbreviations	Brief description
Aspect	AS	Slope orientation
Convergence index	CI	Convergence/divergence index in relation to runoff
Cross sectional curvature	CSC	Measures the curvature perpendicular to the down slope direction
Diurnal anisotropic heating	DAH	Continuous measurement of exposure dependent energy
Flow line curvature	FLC	Represents the projection of a gradient line to a horizontal plane
General curvature	GC	The combination of both plan and profile curvatures
Hill	HI	Analytical hill shading
Hill index	HIINDEX	Analytical index hill shading
Longitudinal curvature	LC	Measures the curvature in the down slope direction
Maximal curvature	MAXC	Maximum curvature in local normal section
Mid-slope position	MSP	Represents the distance from the top to the valley, ranging from 0 to 1
Minimal curvature	MINC	Minimum curvature for local normal section
Morphometric Protection Index	MPI	Measure of exposure/protection of a point from the surrounding relief
Multiresolution index of ridge top flatness	MRRTF	Indicates flat positions in high altitude areas
Multiresolution index of valley bottom flatness	MRVBF	Indicates flat surfaces at bottom of valley
Normalized height	NH	Vertical distance between base and ridge of normalized slope
Plan curvature	PLANC	Described as the curvature of the hypothetical contour line passing through a specific cell
Profile curvature	PROC	Describes surface curvature in the direction of the steepest incline

Terrain attributes	Abbreviations	Brief description
Real surface area	RSA	Actual calculation of cell area
Slope	S	Represents local angular slope
Slope height	SH	Vertical distance between base and ridge of slope
Slope Index	SI	Represents a local angular slope index
Solrad Diffuse1	SolDiffuse1	Insolation Diffuse for the month of January
Solrad Diffuse2	SolDiffuse2	Insolation Diffuse for the month of July
Solrad dur 1	SolDur1	Insolation Duration for the month of January
Solrad dur 2	SolDur2	Insolation Duration for the month of July
Solrad Direct1	SolDiret1	Insolation Direct of month January
Solrad Direct2	SolDiret2	Insolation Direct of the month of July
Solrad Ration1	SolRation1	Ratio between direct Insolation and diffuse Insolation of the month of January
Solrad Ration2	SolRation2	Ratio between direct Insolation and diffuse Insolation of the month of July
Solrad Sunrise1	Sol**Sunrise1**	Mean sunrise time of month January
Solrad Sunrise2	Sol**Sunrise2**	Mean sunrise time of month July
Solrad Sunset1	Sol**Sunset1**	Mean sunset time of month January
Solrad Sunset2	Sol**Sunset2**	Mean sunset time of month July
Solrad total1	SolTotal**1**	Total Insolation for the month of January
Solrad total2	SolTotal**2**	Total Insolation for the month of July
Standardized height	STANH	Vertical distance between base and standardized slope index
Surface specific points	SSP	Indicates differences between specific surface shift points
Tangential curvature	TANC	Measured in the normal plane in a direction perpendicular to the gradient
Terrain ruggedness index	TRI	Quantitative index of topography heterogeneity
Terrain surface convexity	TSC	Ratio of the number of cells that have positive curvature to the number of all valid cells within a specified search radius
Terrain surface texture	TST	Splits surface texture into 8, 12, or 16 classes
Total curvature	TC	General measure of surface curvature
Topographic position index	TPI	Difference between a point elevation with surrounding elevation
Valley depth	VD	Calculation of vertical distance at drainage base level
Valley	VA	Calculation fuzzy valley using the Top Hat approach
Valley Index	VA	Calculation fuzzy valley index using the Top Hat approach
Vector ruggedness measure	VRM	Measures the variation in terrain roughness

Terrain attributes	Abbreviations	Brief description
Topographic wetness index	TWI	Describes the tendency of each cell to accumulate water as a function of relief

205

2.6 Synthetic Soil image (SYSI)

The Synthetic Soil image (SYSI) concept was developed by Demattê et al., (2018). It consists on a multi-temporal bare soil surface images were retrieved from Landsat images during the dry season in Brazil (July to September) between 1984 and 2018. During dry-season the cloud coverage and the soil moisture are reduced, providing higher absolute frequency of bare soil areas on the spectra. Basically the procedure to perform and obtain the SYSI were: *i)* creation of a database with Landsat 5 or Sentinel-2 legacy data.; *ii)* filtering of the database to provide images season in the region; *iii)* insertion of a set of rules into the system to filter other objects besides soils; *iv)* each bare soil occurrence for each location along the time-series was used to calculate a Temporal Synthetic Spectral Reflectance (TESS) of the soil surface; *v)* aggregation of all TESS composes the Synthetic Soil Image (SYSI). This method is further detailed described at Demattê et al., (2018) and correspond to bare soil areas at the soil surface (layer A), designed as Geospatial Soil Sensing System method (GEOS3).

2.7 Principal component analysis and clusterization

Principal component analysis (PCA) was applied to the 7 parameters derived from geophysical sensors data, and the weathering indexes, for each of the 71 collection points. This analysis is a data linear orthogonal transformation, which generates a new set of orthogonal data, called principal components (Cps), which explains the variation of data (Chaplot and Cooper, 2015; Jambu, 1991; Matsuura et al., 2019). Principal components went through a dimensionality reduction process for data grouping. The ideal values of Cps were established by evaluating the *eigenvalues*, where these ideal values are those greater than 1 (>1) (Setiawan et al., 2020; Wang et al., 2018, 2015; Zuber et al., 2017). The ideal number of Cps were three, which were used in the next step.

For cluster analysis, the choice of the ideal number of clusters were performed, based on the homogeneity of the tested groups by statistical *scott* method (Scott and Symons, 1971). This procedure was performed in the *R* software, *fviz_nbclust* function of the "*factoextra*" package (Kassambara and Mundt, 2017). In this manner, three classes were established as the ideal number of clusters. These values were used concomitantly with the three Cps, generated in the previous step, for the definition of groups of similar values of geophysical sensor data, argilluviation and ferralitization indexes. These groups characterize themselves by present similar values within the groups, but different values between one group to another. This processing phase was performed by k-means grouping method, using the "*kmeans*" function in *R* software (R Core Team, 2015).

The information from each sample within each of the three clusters (groups) was concatenated with their respective geographic coordinates. This result was used to extract the values of covariates (morphometric and geological data) at each

sampling point using the *stack* and *extract* functions, respectively, from the "*raster*" package in the *R* software (R Core

235   Team, 2015). The values of each sample within each group were concatenated with the values of the covariates, forming the

base database for entry in the removal by variance process.

2.8 Modeling process

In this research, we tested four machine learning algorithms in modelling process; *Model Averaged Neural Network*

240   (avNNet), *Partial Least Squares* (PLS), *k-Nearest Neighbors* (KKNN) and *Random Forest* (RF). The ideal set of covariates

were used in training the final model of each algorithm. The modelling process were performed in three phases: selection of

covariates, training/testing and spatialization. The general framework is demonstrated in figure 3.
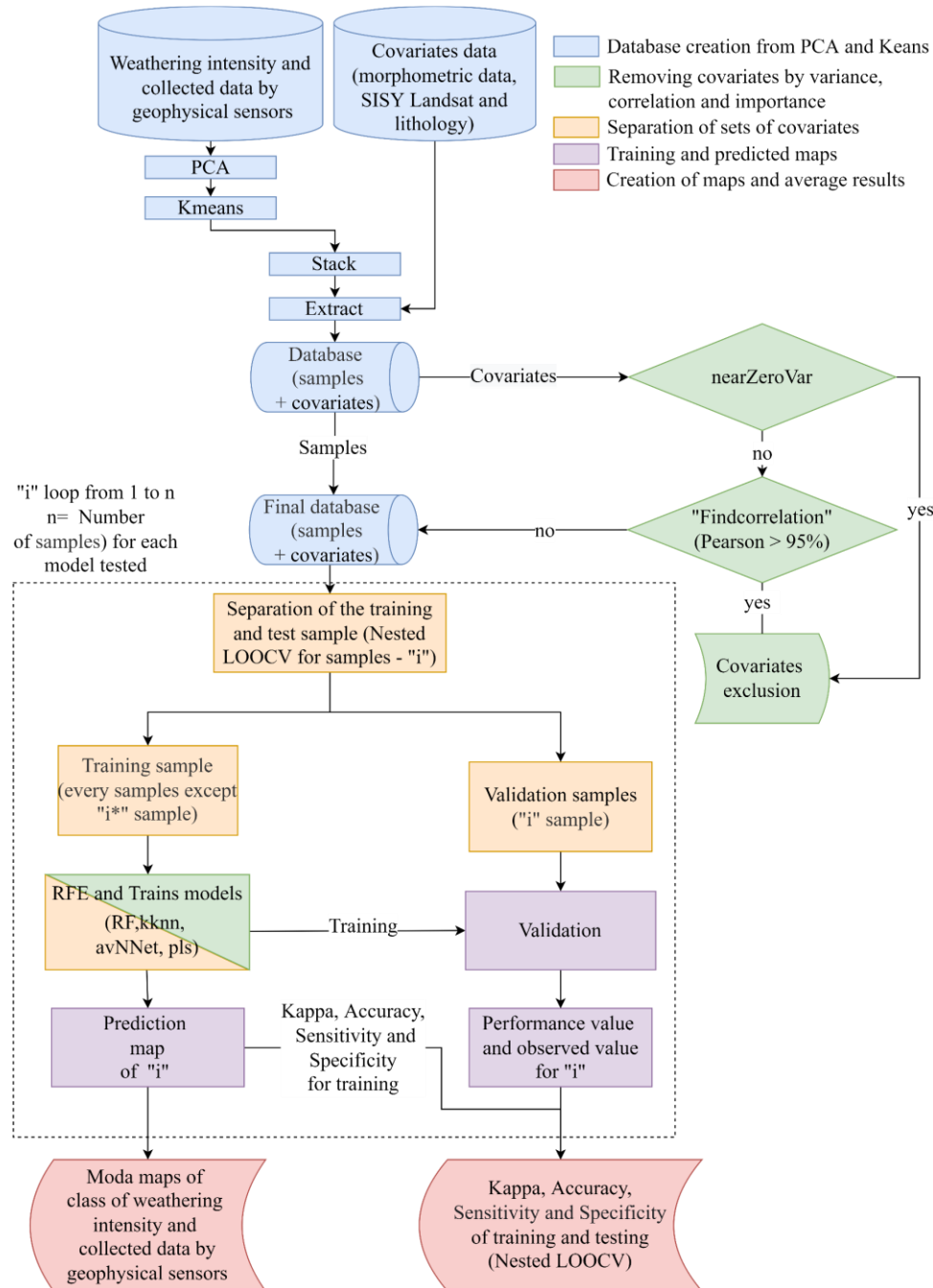
Figure 3. Methodological flowchart showing the sequence of methodologies applied for pedogenetic processes prediction
using geophysical data. The most accurate model between AvNNet: Model Averaged Neural Network; pls: Partial Least
Squares; kknn: k-Nearest Neighbors; RF: Random Forest, were selected to model and map the intensity of pedogenetic
processes maps.

2.8.1 Selection of covariates

The selection of covariates is a procedure that reduces the complexity of the final model (parsimony), reduces computational
250 effort and processing time, and increases the performance of machine processing algorithms (Gomes et al., 2019; Hasri et al.,
2017; Seasholtz and Kowalski, 1993). This procedure is divided into three phases: (1) removal of low-variance covariates
(low variance/close to zero), (2) high correlation removal, and (3) selection by the importance of the covariate.

Phase 1 (removal of low-variance covariates), the values of the covariates at the sampling points are evaluated for
their sample variability. If a covariate presents a variance equal to zero or near zero, it is removed, as it does not contribute to
255 the modeling and demands more processing time in the training of the algorithm. In this analysis, no covariate showed zero
variance. Consequently, all covariates were used in the second phase of selection. The removal of non-variance covariates
was performed using the "nearZeroVar" function from the *Caret* package (Kuhn et al., 2020) in *R* software (R Core Team,
2015).

Phase 2 (high correlation removal), the focus of removal of covariates is made by the correlation between them.
260 Two highly correlated covariates present similar information, one of which can be removed to reduce computational
processing time in the next modeling phases (Darst et al., 2018). This procedure was performed by calculating the *Spearman*
correlation for all covariates, separating pairs of covariates that obtained values greater than 95%. These pairs were evaluated
in relation to the absolute sum of the correlations they have with all the other covariates used, and the covariates that
obtained the highest value in this sum were eliminated. This phase was carried out using the "*find correlation*" function of
265 the "*Caret*" package in the *R* software (Kuhn et al., 2020; R Core Team, 2015). In this step, 9 covariates were
eliminated:"realsurfacearea","slope","solrad_direct1","curv_longitudinal","standardized_height","solrad_diffuse2","curv_cro
ss_secational","solrad_direct2","solrad_ration2". The covariates that were not removed by the previous step, were link
together with the groups predefined by *k-means*.

Phase 3 (removal by importance) is intended to remove those covariates that are less important for the prediction, thus
270 creating a more parsimonious model to explain the phenomenon. In this phase we used the *Recursive Feature Elimination*
method (RFE) (Kohavi and John, 1997). In this step the selection of the optimal subset of predictors was based on *cross-validation* with 10 folds (*repetedcv*), 5 values of each of the internal *hyperparameters* of each tested algorithm (*tuneLenght*).

2.8.2 Separation of training and test of samples

275 The phase of separation, training and test was undertaken using the "nested-leave-one out-cross-validation" ("nested-LOOCV") method (Clevers et al., 2007; Honeyborne et al., 2016; Mello et al., 2022; Rytky et al., 2020). We would like to
emphasize that the sample number of our database is relatively small (71) due to some field limitations. In these cases,
nested-LOOCV is more suitable for performing modelling to which other validation/test methods (as holdout validation)
would not be viable due to the low sample set in the test and/or training group (Ferreira et al., 2021).

280   The nested-LOOCV method comprises a double loop process (inner and outer loops). In the inner loop, the training is performed using a data set of size n-1, using the leave-one-out-cross-validation (LOOCV) for the optimization of the final model. On the other hand, the outer loop corresponds to the test, which the remaining sample is predicted using the final model calculated in the inner loop. This prediction result is stored with the observed value of the remaining sample and later used to calculate the algorithm's performance (Jung et al., 2020; Neogi and Dauwels, 2019). The two loops are run n times

285   (n = total number of samples, in our case 71). All samples are inserted into the outer loop, where the values predicted by the final model of each algorithm are calculated with the predicted and observed values of each sample. Then, the final result of the machine learning algorithm's performance will be obtained by predicted and observed values stored in the external loop.

2.8.3 Training and spatialization of *clusters*

290   For training, all variables selected for each algorithm tested in the previous step were used. In this step, leave-one-out-cross-validation (LOOCV) and 10 repetitions and, 5 values of each internal hyperparameters of each tested algorithm (tuneLength) were used. In the final part of the training, the sample that was not predicted was used for prediction and, the result was used to evaluate the model's performance. The set of samples from the outer loop of the nested-LOOCV method were used for prediction. Five evaluation parameters were used: F-1 Score test (EQ 2), global precision of accuracy (EQ 3), mean

295   sensitivity (EQ 4), mean specificity (EQ 5) and Kappa (EQ 6).

The F1-score is a machine learning parameter that can be used to evaluate classification models (EQ 2). The F1-score test can be defined as the harmonic mean of Precision and Recall (Sasaki, 2007). It is used as a reliable parameter in machine learning techniques for unbalanced data (uneven class distribution). In this sense, it is used to evaluate binary classification systems, which classify examples into 'positive' or 'negative'. Therefore, this score uses false positives and false negatives

300   into account.

$$\text{F} - 1 \text{ Score} = 2 * (Precision . Recall)/(Precision + Recall) \qquad (2)$$

$$\text{F} - 1 \text{ Score} = (T.P)/[(T.P) + \frac{1}{2}(F.P + F.N)]$$

Where:

305   T.P = True positive

F.P = False positive

F.N = False negative

The accuracy indicates the overall performance of the final prediction model, evaluating the number of correct answers of

310   the models, in other words, it indicates the probability that the studied and classified classes correspond to the true data, also presenting values ranging from 0 to 1.

$$Accuracy = \frac{\sum xi}{n} \; x \; 100 \qquad\qquad (3)$$

Where:

xi = sum of all diagonal elements of the confusion matrix

n = total number of samples.

Mean sensitivity is the ability of models to predict the correct values of a class, while average specificity is the ability of models to correct values that are not contained in a class.

$$Sensibility = \frac{\sum_1^n \left(\frac{TP}{TP + FN} \right)}{n} \qquad\qquad (4)$$

$$Specificity = \frac{\sum_1^n \left(\frac{TN}{TN + FP} \right)}{n} \qquad\qquad (5)$$

Where:

TP = number of true positives

FP = false positives

TP = false negatives

n = number of existing classes.

Kappa (K) indices provides a numerical measure and depicts the degree of agreement between the prediction of results and reference values. The kappa indices are used as the basis of the confusion matrix (Morales et al., 2018) (Eq. (4)). The value of K ranges from 0 (no agreement) to 1 (almost perfect) (Landis and Koch, 1977).

$$K = \frac{n \sum_{i=1}^{c} n_{ii} - \sum_{i=1}^{c} n_{i+} + n_{+i}}{n^2 - \sum_{i=1}^{c} n_i + n_{+i}} \qquad\qquad (6)$$

Where:

K = Kappa estimate;

n_{ii} = the value in row i and column i (observed agreement);

n_{i+} = sum of row i, and n + i is the sum of column $_i$ of the confusion matrix (product of the marginals, being the expected agreement);

n = total number of samples;

C = total number of classes.

2.8.3 Generation of final maps and statistics

Selection by the RFE method was repeated 71 times with different training and testing samples. The generated result was analyzed, evaluating the performance parameters of the models (F1-Score test, Kappa, Accuracy, Sensitivity and Sensitivity of each tested algorithm). The prediction error of each algorithm was also analyzed, evaluating the coefficient of variation.

345   Then, the final map was created by combining the 71 prediction maps generated for each algorithm tested. In addition, the mode value for each pixel of the final map was calculated.

The prediction error map was elaborated, considering the number of times that each algorithm chose the mode value in each map pixel normalized by the number of final maps (%).

The nonparametric *Kruskal-Wallis* test (5% significance) was performed to choose the best model and final map. In addition,

350   in relation to accuracy, the *Dunn's posthoc* test was performed to verify statistical differences between the tested algorithms (5% significance). The best final map chosen by the previous statistical tests was used to extract the geophysical sensor data, weathering indexes values at the sampling points.

3. Results and discussion

355   **3.1 Evaluation of model's performance, uncertainty and variables importance**

The models showed varied performance in terms of F1-Score test, kappa, accuracy, sensitivity and specificity (**Table 2**). The best model performance for cluster modelling was RF for evaluating parameters (**Table 2**). Therefore, the RF was selected for the clusters spatialization. Goydaragh et al., (2021) and Assis et al., (2021) also reached satisfactory results using RF for the prediction of different weathering indices using X-ray Fluorescence and RF algorithm to predict weathered regolith

360   thickness, respectively. The RF algorithm presented equivalent performances than other algorithms (Goh et al., 2021; Varga-Szemes et al., 2021). In all tested algorithms the accuracy was not greater than 0.66 (**Table 2**). This probably is due to the small variation of samples or limited distribution of the data set, which reduces the prediction performance in the modelling. Classes with fewer samples tends to present more unstable prediction performances than those with more samples (Zhang and Hartemink, 2020). In addition, according to Johnston et al. (1997) and Lesch et al. 1992) limited number of sampling

365   points or field distribution cannot represent appropriately the spatial variation of soil weathering which would result in low accuracy.

370

Table 2. Model performance in terms of F1-Score test, kappa, accuracy, sensitivity and specificity

Parameter of	Algorithms			
performance	avNNet	kknn	pls	RF
F1-Score test	0.578	0.564	0.472	0.605
Kappa	0.365	0.330	0.278	0.403
Accuracy	0.634	0.0.606	0.606	0.648
Sensitivity	0.566	0.555	0.489	0.596
Specificity	0.781	0.770	0.752	0.797

375 AvNNet: Model Averaged Neural Network; pls: Partial Least Squares; kknn: k-Nearest Neighbors; RF: Random Forest.

The methodological approach optimized the modelling of clusters by applying different geophysical variables plus weathering indexes for assessing prediction uncertainty and spatialization (**Table 2**). The geophysical variables measured in this research are closely associated with weathering processes in more evolved soils, as demonstrated by Pozdnyakov (2008)

380 Mello et al. (2020) and Mello et al. (2021).

For RF algorithm, the sensitivity was 0.60 (**Table 2**). This means that values of sensitivity show moderate performance precision of correctly predict the clusters. Sensitivity corresponds to the observations of a class that were correctly classified as belonging to that class (Brungard et al., 2021). The moderate performance can be explained by different weathering rates within the study area and the tendency of models to be a generalist and predict areas homogeneously. In this way, some

385 samples collected within that region are grouped into another class that the machine learning algorithm does not predict. In this sense, some collected points within the same cluster show results from different clusters.

The specificity for RF was 0.80 (**Table2**). This indicates that values of sensitivity presented a satisfactory performance and correctly predict the clusters. Specificity is complementary to sensitivity and, it corresponds to the observations not in that class that was correctly classified as not RF algorithm was able to adequately estimate the values of the classes from the data

390 collected in the field. For both, sensitivity and specificity our values are slightly lower than those found by Kodikara and McHenry, (2020) in which all models achieved 80% or higher sensitivity and specificity, to determine the physical and mineralogical properties of lunar soil using small soil dataset.

The importance of covariates in predicting and spatializing clusters showed that the SYSI and terrain surface convexity (TSC) were the most important variables to cluster by RF model, contributing more than 75% to the decreasing of the mean

395 accuracy, while the digital elevation model (DEM) contributed in 50%, (**Fig. 4**).
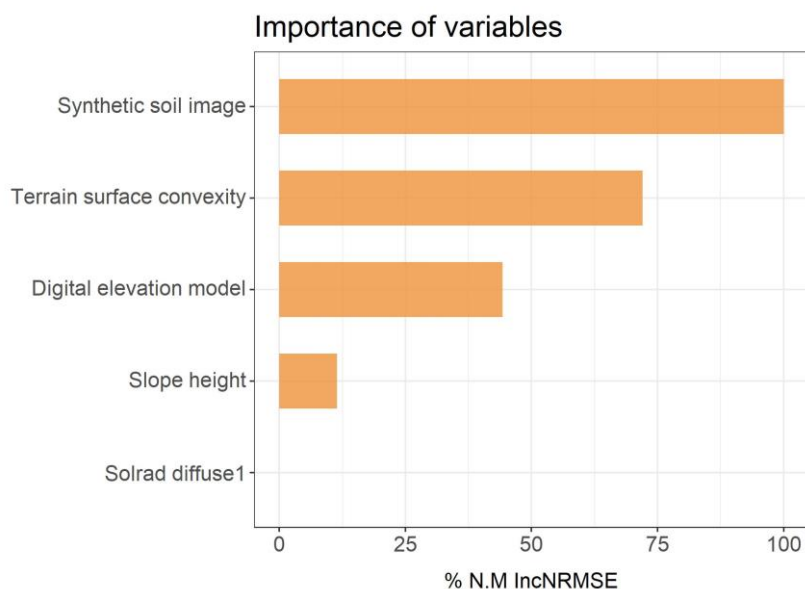
Figure 4. Variable importance of predictors. %N.M IncRMSE: Normalized Mean Increment of RMSE - how much in % each variable contribute in modelling process.

400   The Synthetic Soil Image (SYSI) (**Fig. 4**) approach is able to identify and characterize soil texture (clay, silt and sand content) at the image level (Fongaro et al., 2018). In this sense, the silt/clay ratio are correlated to the weathering index once Ferralsols/Nitisols present low values, while Regosols/Cambisols present higher values due to their high and low degree of weathering respectively (Dos Santos et al., 2018). Also, the SYSI is strongly correlated with SiO_2 and Al_2O_3 contents (Fioriob, 2013). Which is the basic information to calculate the *ki* ($ki = SiO_2/Al_2O_3 \times 1.7$) a tropical weathering index (Dos

405   Santos et al., 2018). Despite these, Silvero et al., (2021) detected soil color using SYSI which is also related with soil mineralogical composition, mainly iron oxides related to the weathering index. Also, the SYSI has this ability because it has wavelengths from visible to NIR and SWIR where intensities could be related to some minerals (e.g. soil minerals, hematite, quartz, ilmenite, and others) (Demattê et al., 2018). The SiO_2 to Al_2O_3 ratios are used to calculate other weathering indexes for Brazilian tropical soils (Dos Santos et al., 2018). Thus, SYSI brings strong physical information related to several soil

410   properties and inference with soil weathering.

Terrain surface convexity (TSC; **Fig. 4**) controls the amount of water that infiltrates and/or runs off the terrain surface (Burt and Butcher, 1985). Areas with null and/or negative values are prone to infiltration and, areas with positive values have reduced infiltration. These conditions associated with areas of free drainage (i.e., no impeded drainage) favor and increase the action of hydrolysis and, consequently, chemical weathering (Osher and Buol, 1998; Schaetzl and Anderson, 2005),

415   which operates at different rates.

Digital elevation model (**Fig. 4**) is related to some relief variables (e. g., topographic wetness index, terrain ruggedness index and slope) and has a similar effect to terrain surface convexity in controlling water dynamic at the different landscape positions, which in turn controls the intensities of weathering processes (McBratney et al., 2003).

420 **3.2 Differences between clusters and the relationship with lithology, soil types and weathering rates**

The area over east diabase (cluster 3) showed greater intensity of weathering when compared to the area over west diabase (cluster 1) (**Fig. 5**). This indicates that weathering is operating at different intensities in the same lithology. The difference between the weathering intensities on both diabase areas is not expected, once the area is small and variations in the mineralogical composition of diabase are not expected (Mello et al., 2020). Our results disagree with those found by
425 Banerjee and Chakrabarti, (2018), who explained the different weathering indexes by the selective weathering of the rock-forming minerals in the weathered diabase. Nevertheless, Santos et al., (2021) stated that soil over diabase areas can be formed under environmental conditions that favoured more the weathering of primary minerals and neoformation of minerals in some particular area. In our study site, the condition that favoured the greater weathering of diabase primary minerals in cluster 3 (East diabase) compared to cluster 1 (Est diabase) (**Fig. 5**) probably were the differences in topographic
430 position and some terrain attributes (**Table 1**). In addition, the diabase mineralogical composition (mostly composed of ferromagnesian minerals) favors high intensities of weathering under a tropical climate (Breemen and Buurman, 2003; Colman, 1982; Eggleton et al., 1987), such as diabase areas.
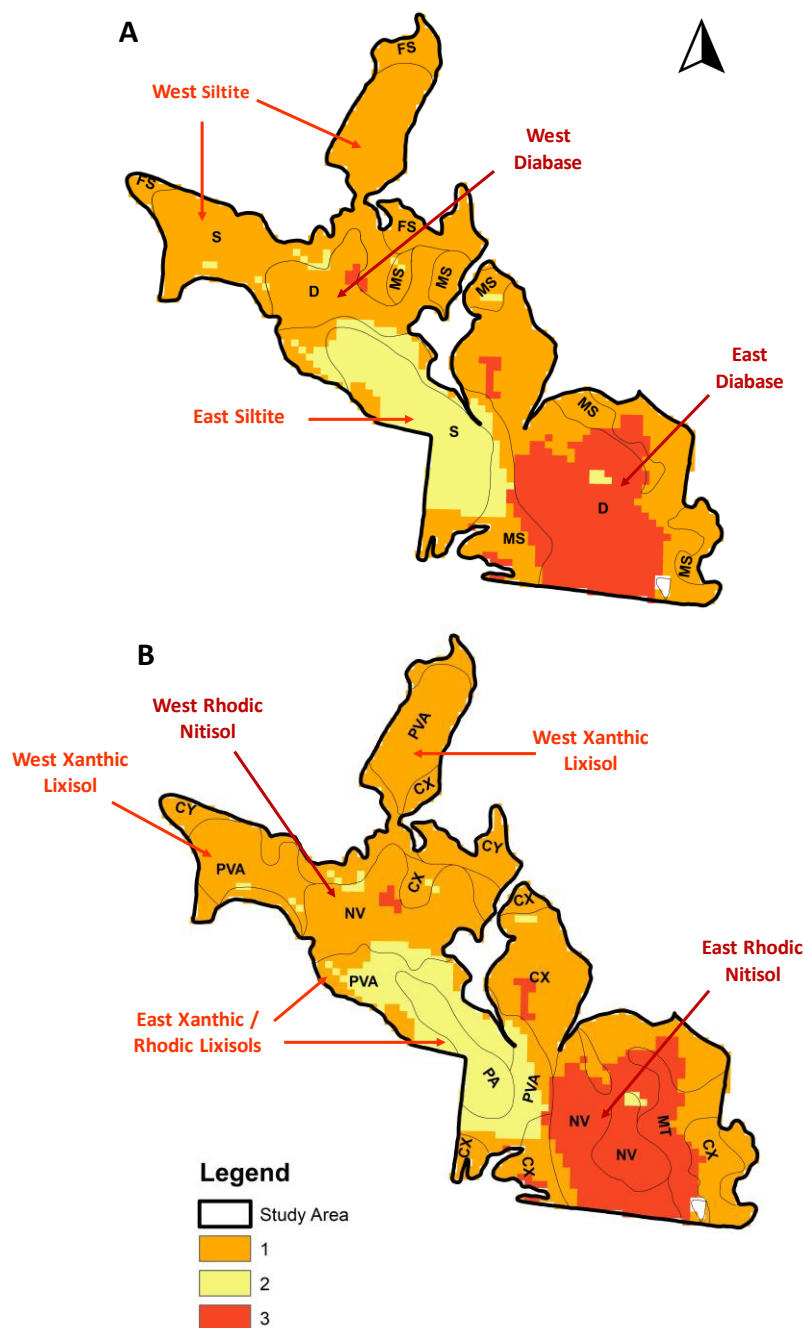
Figure 5. The figure shows the relationship between clusters - lithology – weathering intensities. **A**: Clusters indicating the
intensity of weathering over the different lithologies: D - Diabase; MS - Metamorphosed siltite; S - Siltite: FS - Fluvial
Sediments. **B**: Clusters indicating the intensity of weathering on the different types of soils: CX: Haplic Cambisols, CY:
Fluvic Cambisols, MT: Luvic Phaozem, NV: Rhodic Nitisol: PA: Xanthic Acrisol, PVA: Rhodic Lixisol.

The area over West and East siltites (clusters 1 and 2, respectively) showed significant differences in weathering rates (**Fig.**
5). West siltite presented greater weathering rates compared to East siltite. This also indicates different weathering rates
operating over siltite areas. The different in weathering intensity can also be attributed to the differences topographic
position and some terrain attributes as slope and terrain ruggedness index (**Table 1**), once significant mineralogical
variations in siltite are not expected in such small areas. West siltite lies over a flatter topographical position and in a lower
part of the landscape which favors infiltration, hydrolysis and, thus, higher intensities of chemical weathering processes,
fueled by higher water activities and the dilute weathering solutions. On the other hand, East siltite are located on highest
position of the steepest relief which hampers water infiltration. In addition, under extreme weathering conditions (cluster 1 –
West siltite) the relationship between Titanium and other elements like Aluminium and Silicon in the upper parts of soil
profiles (i.e., most weathered) tends to show an increase in Titanium contents due to preferential removal of Al-rich phases
(Young and Nesbitt, 1998). As a result, the relationship used to calculate the weathering index (W1 = SiO_2/TiO_2 * 100; Eq.
(1)) is altered and reflected in clusterization processes.

East Rhodic Nitisol (cluster 3) showed a higher weathering index (more weathered soil) when compared to west Rhodic
Nitisol (cluster 1; less weathered soil) and an intermediate weathering index over cluster 2 (moderated weathered soil) (**Fig.**
5). These differences also indicate that the weathering is probably operating at different rates in these soils. The
rock/saprolite transformation is replaced upwards by weathering (Fritsch and Fitzpatrick 1994), under favorable
environmental conditions, such as free drainage, high pluviosity, rich iron parent material and flat relief position
(Schwertmann, 1988; Breemen and Buurman, 1998). All these environmental conditions are found and are homogeneous
over the Rhodic Nitisol area, except topographic position and terrain attributes. East Rhodic Nitisol is located at a more flat
and high landscape position compared to West Rhodic Nitisol. The environmental condition on West Rhodic Nitisol favors
water infiltration, hydrolyses and, thus, silica and basic cations removal. In this sense, variation in topographic position and
terrain attributes can explain the variation in weathering index in terms of soil.

The Rhodic and Xanthic Lixisols (clusters 1 and 2) presented different weathering intensities (**Fig. 5**). The West Rhodic
Lixisols (cluster 1) showed the highest weathering intensities, whereas the East Xanthic and Rhodic Lixisols showed the
lower weathering intensities (**Fig. 5**). The explanation is related to the argilluviation processes in these types of soils, which
is intensified according to weathering rates (Schaetzl and Anderson, 2005).

The statistical analysis (*Kruskal-Wallis* test) (**Table 3**) support our results and discussion above. For weathering, there were
differences between clusters 1, 2 and, class 3. In practical and interpretative aspects, the highest weathering intensities
occurred in ascending order: clusters 2, 1 and 3, respectively, over the different lithologies and soil types associated, (**Fig. 5**).

Table 3. Statistical analysis for the three clusters, for the weathering plus geophysical variables by the *Kruskal-Wallis*

Clusters	eU (ppm)	eTh (ppm)	K^{40}	Magnetic susceptibility	ECa	Weathering Index
1	2.85 a	7.61 a	0.45 a	17.32 a	5.81 a	1021.7 a
2	2.54 ab	5.04 b	0.22 b	6.33 b	7.29 a	2236.9 b
3	2.08 b	6.75 ab	0.28 ab	74.27 c	-46.6 b	574.5 c

3.3 The influence of pedogeomorphology and geophysical variables on clusterization

475   Figure 6 demonstrates how clusters are distributed on the landscape under the influence of relief (i.e., slope and topographic position). Relief acts directly on weathering by controlling water infiltration and dynamics on (and within) the soil; i.e., surface runoff and infiltration rates (Jackson, 1957; Schaetzl and Anderson, 2005).

A

B
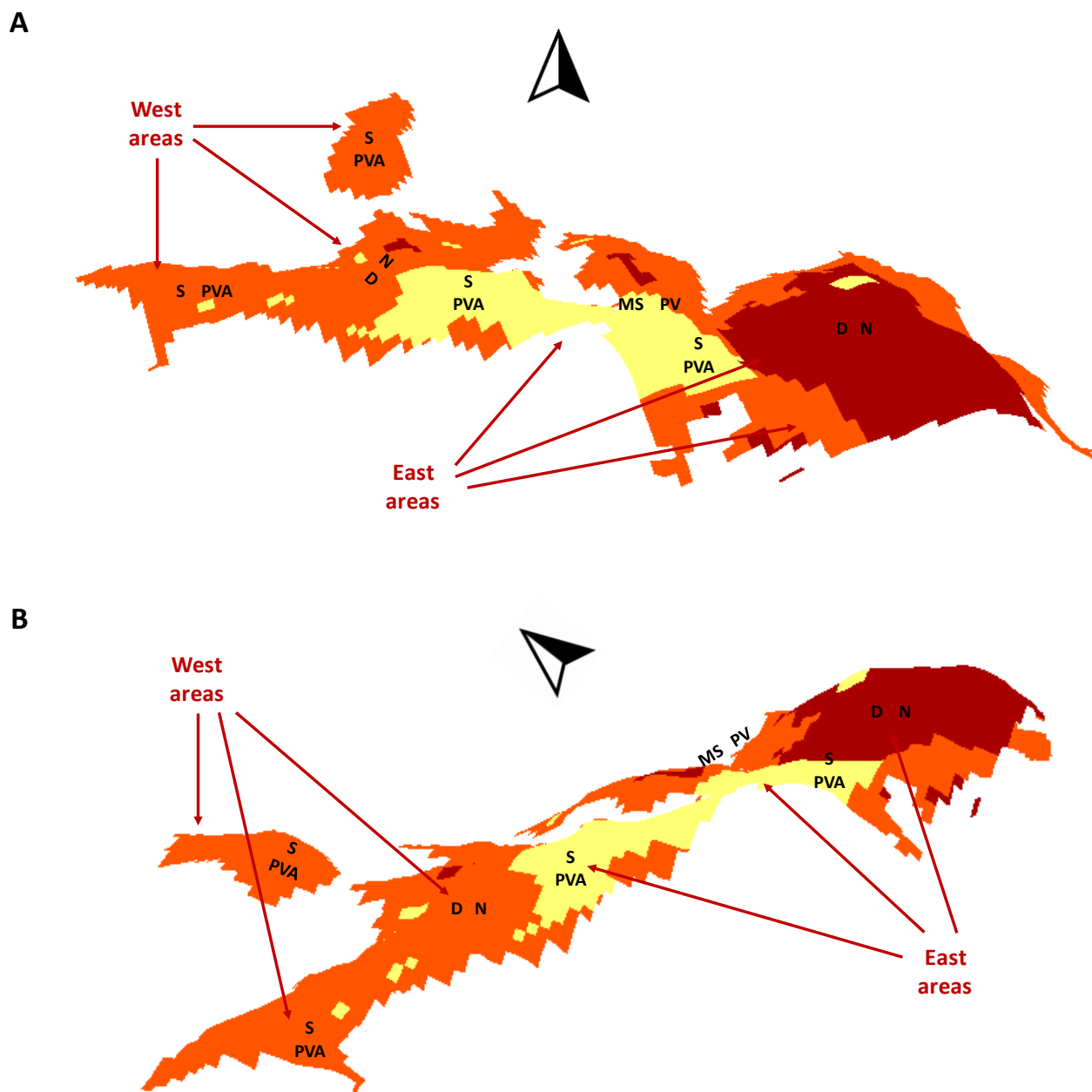
Figure 6. A and B: The figures demonstrated the relationship between pedogeomorphology and clusters for different weathering intensities. The variation of the weathering intensity indicated by the clusters on the different topographic positions in the landscape and relief features under different views. Soil classes: D: Diabase, MS: Metamorphosed siltite, S: Siltite. CX: Haplic Cambisols, CY: Fluvic Cambisols, MT: Luvic Phaozem, NV: Rhodic Nitisol: PA: Xanthic Acrisol, PVA: Rhodic Lixisol.

485

For the weathering intensities over East and West diabase, as well as for the Rhodic Nitisol over this lithology, the single difference among pedoenvironmental variables were in the terrain attribute (terrain surface convexity and topographic position associated to DEM; **Fig. 6**). For the higher weathering rates (cluster 3; **Fig. 6**), the East areas are located at the

490   hilltop and at a flat relief, which favors water infiltration, leaching and a more efficient hydrolysis, and thus, a more intense chemical weathering. As a result, silica is removed throughout soil profile (i.e., desilication) leading to the residual concentration of kaolinite (monosialitization) (Samotoin and Bortnikov, 2011) and residual concentration of iron oxides (ferralitization) (Ker et al., 2015), corroborating the greater weathering rates. For cluster 1, over diabase east (**Fig. 6**), there is a slight slope, which causes a reduction in water infiltration, chemical weathering and consequently, in desilication. The

495   diabase West area and Rhodic Nitisol (cluster 1) are located at low topographic positions (**Fig. 6**), but a slope slightly greater than the relief on cluster 3, which in turn affects the terrain surface convexity and slope. Therefore, the infiltration and chemical weathering are reduced, and consequently, the weathering intensities which explains the lower values for the weathering indexes over this area.

The Rhodic Lixisols over West siltite (cluster 1) presented the higher weathering intensities, when compared to Rhodic /

500   Xanthic Lixisols (cluster 2) (**Fig. 6**). The greater weathering intensities for areas over cluster 1 are related to the flat relief and low topographic position. The combination of these terrain attributes favors a greater water inflow from the highest parts of the landscape and more water infiltration. As a result, both weathering and leaching (i.e., removal of soluble elements) are intensified (Breemen and Buurman, 2003; Dalsgaard et al., 1981; Schaetzl and Anderson, 2005). On the other hand, the Rhodic / Xanthic Lixisols over Est siltite (cluster 2) presented the lower weathering rates. This area is located at a hill slope

505   in the landscape. Our results agree with Modenesi, (1983) who stated that in hillslopes weathering is more related to morphogenetic dynamics. Steep slopes increase the rate of surface erosion and decrease the rate of infiltration and lateral subsurface water flow (Schaetzl and Anderson, 2005), which reduces the chemical weathering.

Weathering also affected the geophysical parameters (κ, eU, eTh, K^{40} and ECa) in different ways, resulting in differences according to the intensity of this process in more evolved and weathered soil types (Rhodic Nitisols, Rhodic and Xanthic

510   Lixisols) **(Fig. 5 - Table 3)**.

For κ (**Table 3**), weathering in Rhodic Nitisols determine the distribution of ferrimagnetic minerals in the soil profile, due to the residual accumulation of iron oxides (Driessen et al., 2001), which directly affects κ (Mello et al., 2020). Indeed, mafic igneous rocks such as diabase, are rich in ferrimagnetic minerals (Aydin et al., 2007), which through weathering, release iron into the soil profile (Cervi et al., 2019; De Jong et al., 2000). Under drainage free and hot environments, iron reprecipitates

515   as ferrimagnetic minerals (Grimley and Vepraskas, 2000; Maxbauer et al., 2016), which are also good weathering degree indicators.

The radionuclides eU, eTh, K^{40} contents (**Table 3**) are affected by weathering (Mello et al., 2021; Wilford, 2012; Wilford et al., 1997). During weathering in Rhodic Nitisols over diabase areas, originating from mafic parent materials on stable

geomorphic surfaces, flat relief and deeply weathered soils, the K^{40} is leached and eU and eTh are adsorbed by clay and iron
520   oxides in the nitic B horizon (Dickson and Scott, 1997; Viscarra Rossel et al., 2014). Similarly, in Rhodic and Xanthic
Lixisols (Est siltite - cluster 2) (**Table 3**) weathering and argilluviation lead to a clay accumulation at the B horizon (argic
horizon). As a result, there is a greater adsorption of eU and eTh onto clay minerals in the argic horizon (Dickson and Scott,
1997; Syed, 1999; Vandenhove et al., 2007; Santos-Francés et al., 2018).

Weathering affects soil ECa values (**Table 3**). Chemical weathering processes (in association with pedogenetic processes)
525   affects different soil attributes (e.g., texture, CEC, porosity, bulk density and water retention). These attributes govern the
ECa values (Mcneill, 1992; Rhoades et al., 1999a; Sudduth et al., 2001). Intense weathering leads to ferralitization in Rhodic
Nitisol (**Fig. 5**) resulting in the development of a good structure and porosity and depth soils (Breemen, and Buurman,
2003), where the ECa values reflect the greater effective soil depth (Peralta et al., 2013). On the other hand, weathering
associated to parent material and relief characteristcs leads to argilluviation in Rhodic and Xanthic Lixisols (**Fig. 5**) results in
530   accumulation of clay in soil subsurface, changing hidraulic conductivity and soil depth , which strongly affect ECa values
Taylor et al., (2009), due to keep more humidity and íons in soil solution. In addition, the higher clay content result in high
specific surface area of the clays, basic cation and water retention and consequently high ECa values (Corwin and Lesch,
2005; Fritz et al., 1999; Hepper et al., 2006; Osher and Buol, 1998; Saidian et al., 2015).

535   **4. Conclusions**

The RF algorithm presented the satisfactory and better performance to model the clusters corresponding to the different
intensities weathering in terms of F1-score, kappa, accuracy, sensibility and sensitivity. This algorithm was able to
satisfactorily identify different intensities of weathering, using as input data geophysical soil variables, calculated weathering
indexes and terrain attributes. The nested-LOOCV methods proved to be adequate for modeling weathering intensity,
540   associated with geophysical sensors for a small dataset and, nested-LOOCV was a robust method to evaluate the algorithm's
performance, allowing the optimisation and increasing the efficiency of training and testing of models.

The environmental geophysical variables used (κ, eU, eTh, K^{40} and ECa) were related and affected by weathering, which
effectively contributed to modelling and clusterization processes to identify different weathering intensities.

The SYSI, TSC and DEM were the most important variables to modelling and identifying the different weathering
545   intensities. This suggests that the different weathering intensities are mainly modulated by geomorphic processes, which
affect soil surface reflectance once the other soil-forming factors are the same.

Our analysis by geophysical data and machine learning algorithm revealed that the weathering is operating at different
intensities both on the diabase/Rhodic-Nitisols and the siltite/metasiltite – Rhodic and Xanthic Lixisols areas. At the former,
highest intensities of the process occur on Nitisol in the east area and the smaller intensities occur on Nitisol in the west area.
550   At the latter, the highest intensities occur in the west Xanthic Lixisols and, the lowest intensities of that processes occur on
the Rhodic and Lixisols in the east area.

Relief and topographic position controls water dynamic at the landscape and directly affects the weathering intensities. This was evidenced in the same soil types, originated from the same parent material, however, allocated in different positions at the landscape.

555 The different weathering intensities have applicability in understanding geomorphic processes and weathering at various spatial and temporary scales in the landscape and also in mapping of soil attributes. However, it is important to highlight that the characteristics of the input dataset in the models can be a limitation for the technique. The use of a greater number of associated and additional covariates, (e.g., landscape position and climate), has the potential to improve the estimation of the weathering intensities.

560

5. Authors contribution

Danilo César de Mello: conceived of the presented idea, carried out the experiment, developed the theoretical formalism, contributed to the design and implementation of the research, to the analysis of the results and to the writing of the

565 manuscript. He provided critical feedback and helped shape the research, analysis and manuscript.

Tiago Osório Ferreira: conceived of the presented idea. developed the theoretical formalism, contributed to the design and implementation of the research, to the analysis of the results and to the writing of the manuscript. He provided critical feedback and helped shape the research, analysis and manuscript.

570

Gustavo Vieira Veloso: designed the model and the computational framework and analysed the data, planned and carried out the simulations, performed the analytic calculations and performed the numerical simulations, modelling processing, evaluate algorithms performance, variables importance and statistical analyses.

575 **Marcos Guedes de Lana:** contributed to the interpretation of the results, took the lead in writing the manuscript. Devised the project, the main conceptual ideas and proof outline. He worked out almost all of the technical details. All authors provided critical feedback and helped shape the research, analysis and manuscript.

Fellipe Alcantara de Oliveira Mello: contributed to the interpretation of the results, took the lead in writing the manuscript.

580 All authors provided critical feedback and helped shape the research, analysis and manuscript.

Luis Augusto Di Loreto Di Raimo: performed the analysis, drafted the manuscript and designed the figure. All authors provided critical feedback and helped shape the research, analysis and manuscript.

585 **Diego Ribeiro Oquendo Cabrero:** performed the analysis, drafted the manuscript and designed the figure. All authors provided critical feedback and helped shape the research, analysis and manuscript.

José João Lelis Leal de Souza: Critical revision of the article. All authors discussed the results and commented on the manuscript. He contributed to the interpretation of the results and verified the analytical methods.

590

Elpídio Inácio Fernandes Filho: Critical revision of the article. He designed the model and the computational framework and analysed the data. He contributed to the interpretation of the results and verified the analytical methods. All authors discussed the results and commented on the manuscript.

595 **Márcio Rocha Francelino:** contributed to the interpretation of the results, took the lead in writing the manuscript. All authors provided critical feedback and helped shape the research, analysis and manuscript.

Carlos Ernesto Gonçalves Reynaud Schaefer: contributed to the interpretation of the results, took the lead in writing the manuscript. All authors provided critical feedback and helped shape the research, analysis and manuscript.

600

José Alexandre Melo Demattê: Provided de financial support, leadership of the group, critical revision of the article. He contributed to the interpretation of the results and verified the analytical methods. Encouraged the co-authors to investigate a specific aspect and supervised the findings of this work.

605 **6. Code and data availability**

All codes and data from this research will be made available in the Zenodo repository, with its own DOI, after the review process in "R software", as well as their respective packages and versions will be listed in the database and codes available in the data_base.zip in the indicated repository.

610 **7. Acknowledgements**

We would like to thank the National Council for Scientific and Technological Development (CNPq) for the first author's scholarship (grant No. 134608/2015-1; grant number 305996/2018-5); the São Paulo Research Foundation (FAPESP) (grant No. 2014-22262-0) for providing essential resources to the Laboratory of Remote Sensing Applied to Soils from the "Luiz de Queiroz" College of Agriculture (ESALQ/USP); This study was financed in part by the Coordenação de Aperfeiçoamento

615 de Pessoal de Nível Superior - Brazil (CAPES) - Finance Code 001"; Also, we thanks the Geotechnologies in Soil Science group (GeoSS – website http://esalqgeocis.wixsite.com/english) and LabGeo – UFV - 'Programa de Pós-Graduação em Solos e Nutrição de Plantas – PGSNP' of the Soil Department of the Universidade Federal de Viçosa, Brazil and the Institute of Geosciences at Campinas State University, Brazil, for their support.

620

8. References

Alvares, C. A., Stape, J. L., Sentelhas, P. C., De Moraes Gonçalves, J. L. and Sparovek, G.: Köppen's climate classification map for Brazil, Meteorol. Zeitschrift, 22(6), 711–728, doi:10.1127/0941-2948/2013/0507, 2013.

625 Anderson, S. P., Blum, J., Brantley, S. L., Chadwick, O., Chorover, J., Derry, L. A., Drever, J. I., Hering, J. G., Kirchner, J. W., Kump, L. R., Richter, D. and White, A. F.: Proposed initiative would study earth's weathering engine, Eos (Washington. DC)., 85(28), 2–7, doi:10.1029/2004EO280001, 2004.

Apollaro, C., Perri, F., Borrelli, L. and Caloiero, T.: Editorial The Role of Water-Rock Interaction Processes in Soil Formation: Geochemical, Mineralogical, Geomorphological, and Engineering- Geological Aspects, 2019(October 2017), 630 2019.

Assis, L. M., Francelino, M. R., Daher, M., Fernandes-Filho, E. I., Veloso, G. V., Gomes, L. C. and Schaefer, C. E. G. R.: Modeling regolith thickness in iron formations using machine learning techniques, CATENA, 207, 105629, doi:https://doi.org/10.1016/j.catena.2021.105629, 2021.

Aydin, A., Ferré, E. C. and Aslan, Z.: The magnetic susceptibility of granitic rocks as a proxy for geochemical composition: 635 Example from the Saruhan granitoids, NE Turkey, Tectonophysics, 441(1–4), 85–95, doi:10.1016/j.tecto.2007.04.009, 2007.

Ayoubi, S., Abazari, P. and Zeraatpisheh, M.: Soil great groups discrimination using magnetic susceptibility technique in a semi-arid region, central Iran, Arab. J. Geosci., 11(20), doi:10.1007/s12517-018-3941-4, 2018.

Bai, W., Kong, L. and Guo, A.: Effects of physical properties on electrical conductivity of compacted lateritic soil, J. Rock Mech. Geotech. Eng., 5(5), 406–411, doi:10.1016/j.jrmge.2013.07.003, 2013.

640 Banerjee, A. and Chakrabarti, R.: Large Ca stable isotopic (δ44/40Ca) variation in a hand-specimen sized spheroidally weathered diabase due to selective weathering of clinopyroxene and plagioclase, Chem. Geol., 483, 295–303, doi:https://doi.org/10.1016/j.chemgeo.2018.02.031, 2018.

Bazaglia Filho, O., Rizzo, R., Lepsch, I. F., Prado, H. do, Gomes, F. H., Mazza, J. A. and Demattê, J. A. M.: Comparison between detailed digital and conventional soil maps of an area with complex geology, Rev. Bras. Ciência do Solo, 37(5), 645 1136–1148, doi:10.1590/s0100-06832013000500003, 2013.

Beamish, D.: Gamma ray attenuation in the soils of Northern Ireland, with special reference to peat, J. Environ. Radioact., 115, 13–27, doi:10.1016/j.jenvrad.2012.05.031, 2013.

Beamish, D.: Relationships between gamma-ray attenuation and soils in SW England, Geoderma, 259–260, 174–186, doi:10.1016/j.geoderma.2015.05.018, 2015.

650 Bland, Will; Rolls, D.: Weathering: An introduction to the scientific principles, edited by A. Routledge., 2016.

Borrelli, L., Perri, F., Critelli, S. and Gullà, G.: Catena Characterization of granitoid and gneissic weathering pro fi les of the Mucone River basin (Calabria , southern Italy), Catena, 113, 325–340, doi:10.1016/j.catena.2013.08.014, 2014.

Borrelli, L., Critelli, S., Gullà, G., Muto, F., Borrelli, L., Critelli, S., Gullà, G. and Muto, F.: Weathering grade and geotectonics of the western-central Mucone River basin (Calabria , J. Maps, 0(0), 1–19, doi:10.1080/17445647.2014.933719, 2015.

Borrelli, L., Coniglio, S., Critelli, S., Barbera, A. La, Borrelli, L., Coniglio, S., Critelli, S. and Barbera, A. La: Weathering grade in granitoid rocks : The San Giovanni in Fiore area (Calabria , Italy), , 5647, doi:10.1080/17445647.2015.1010742, 2016.

Brantley, S. L., Megonigal, J. P., Scatena, F. N., Balogh-Brunstad, Z., Barnes, R. T., Bruns, M. A., Van Cappellen, P., Dontsova, K., Hartnett, H. E., Hartshorn, A. S., Heimsath, A., Herndon, E., Jin, L., Keller, C. K., Leake, J. R., Mcdowell, W. H., Meinzer, F. C., Mozdzer, T. J., Petsch, S., Pett-Ridge, J., Pregitzer, K. S., Raymond, P. A., Riebe, C. S., Shumaker, K., Sutton-Grier, A., Walter, R. and Yoo, K.: Twelve testable hypotheses on the geobiology of weathering, Geobiology, 9(2), 140–165, doi:10.1111/j.1472-4669.2010.00264.x, 2011.

Breemen, Nico and Buurman, P.: Soil Formation, 2 nd., Laboratory of Soil Science and Geology, New YorkK, Boston, Dordrecht, London, Moscow., 2003.

van Breemen, N. and Buurman, P.: Ferralitization, Soil Form., 291–312, 1998.

Brenning, A.: Statistical geocomputing combining R and SAGA: The example of landslide susceptibility analysis with generalized additive models, Hamburg. Beiträge zur Phys. Geogr. und Landschaftsökologie, 19(23–32), 410, 2008.

Burt, T. P. and Butcher, D. P.: Topographic controls of soil moisture distributions, J. Soil Sci., 36(3), 469–486, 1985.

Buss, H. L., Chapela Lara, M., Moore, O. W., Kurtz, A. C., Schulz, M. S. and White, A. F.: Lithological influences on contemporary and long-term regolith weathering at the Luquillo Critical Zone Observatory, Geochim. Cosmochim. Acta, 196, 224–251, doi:10.1016/j.gca.2016.09.038, 2017.

Cabral Pinto, M. M. S., Silva, M. M. V. G., Ferreira da Silva, E. A., Dinis, P. A. and Rocha, F.: Transfer processes of potentially toxic elements (PTE) from rocks to soils and the origin of PTE in soils: A case study on the island of Santiago (Cape Verde), J. Geochemical Explor., 183(August 2016), 140–151, doi:10.1016/j.gexplo.2017.06.004, 2017.

Camargo, O.A.; Moniz, A.C.; Jorge, J.A. & Valadares, J. M. A. S.: Métodos de análise química, mineralógica e física de solos do Instituto Agronômico do estado de São Paulo, Bol. técnico, 106, 94, 1986.

Camargo, L. A., Marques Júnior, J., Pereira, G. T. and Bahia, A. S. R. de S.: Clay mineralogy and magnetic susceptibility of Oxisols in geomorphic surfaces, Sci. Agric., 71(3), 244–256, doi:10.1590/S0103-90162014000300010, 2014.

Cardoso, R. and Dias, A. S.: Study of the electrical resistivity of compacted kaolin based on water potential, Eng. Geol., 226(January), 1–11, doi:10.1016/j.enggeo.2017.04.007, 2017.

Carroll, D.: Rock weathering, Springer Science & Business Media., 2012.

Cervi, E. C., Maher, B., Poliseli, P. C., de Souza Junior, I. G. and da Costa, A. C. S.: Magnetic susceptibility as a pedogenic proxy for grouping of geochemical transects in landscapes, J. Appl. Geophys., 169, 109–117, doi:10.1016/j.jappgeo.2019.06.017, 2019.

César de Mello, D., Demattê, J. A. M., Silvero, N. E. Q., Di Raimo, L. A. D. L., Poppiel, R. R., Mello, F. A. O., Souza, A. B., Safanelli, J. L., Resende, M. E. B. and Rizzo, R.: Soil magnetic susceptibility and its relationship with naturally occurring processes and soil attributes in pedosphere, in a tropical environment, Geoderma, 372, doi:10.1016/j.geoderma.2020.114364, 2020.

690 Chaplot, V. and Cooper, M.: Soil aggregate stability to predict organic carbon outputs from soils, Geoderma, 243, 205–213, 2015.

Chung, C., Lin, C., Yang, S., Lin, J. and Lin, C.: Investigation of non-unique relationship between soil electrical conductivity and water content due to drying-wetting rate using TDR, Eng. Geol., 252(March 2018), 54–64, doi:10.1016/j.enggeo.2019.02.025, 2019.

695 Clevers, J. G. P. W., Van Der Heijden, G. W. A. M., Verzakov, S. and Schaepman, M. E.: Estimating grassland biomass using SVM band shaving of hyperspectral data, Photogramm. Eng. Remote Sensing, 73(10), 1141–1148, doi:10.14358/PERS.73.10.1141, 2007.

Colman, S. M.: Chemical weathering of basalts and andesites, 1982.

Corwin, D. L. and Lesch, S. M.: Apparent soil electrical conductivity measurements in agriculture, Comput. Electron. 700 Agric., 46(1–3), 11–43, 2005.

Corwin, D. L., Lesch, S. M., Shouse, P. J., Soppe, R. and Ayars, J. E.: Identifying Soil Properties that Influence Cotton Yield Using Soil Sampling Directed by Apparent Soil Electrical Conductivity, , (1995), 352–364, 2003.

Dalsgaard, K., Baastrup, E. and Bunting, B. T.: The influence of topography on the development of Alfisols on calcareous clayey till in Denmark, Catena, 8(2), 111–136, 1981.

705 Darst, B. F., Malecki, K. C. and Engelman, C. D.: Using recursive feature elimination in random forest to account for correlated variables in high dimensional data, BMC Genet., 19(1), 65, 2018.

Demattê, J. A. M., Fongaro, C. T., Rizzo, R. and Safanelli, J. L.: Geospatial Soil Sensing System (GEOS3): A powerful data mining procedure to retrieve soil spectral reflectance from satellite images, Remote Sens. Environ., 212(August 2017), 161–175, doi:10.1016/j.rse.2018.04.047, 2018.

710 Dickson, B. L. and Scott, K. M.: Interpretation of aerial gamma-ray surveys - adding the geochemical factors, AGSO J. Aust. Geol. Geophys., 17(2), 187–200, 1997.

Doetterl, S., Berhe, A. A., Arnold, C., Bodé, S., Fiener, P., Finke, P., Fuchslueger, L., Griepentrog, M., Harden, J. W., Nadeu, E., Schnecker, J., Six, J., Trumbore, S., Van Oost, K., Vogel, C. and Boeckx, P.: Links among warming, carbon and microbial dynamics mediated by soil mineral weathering, Nat. Geosci., 11(8), 589–593, doi:10.1038/s41561-018-0168-7, 715 2018.

Driessen, P., Deckers, J., Spaargaren, O. and Nachtergaele, F.: Lecture notes on the major soils of the world, No. 94., edited by R. World Soil Resources Reports , FAO, World Soil Resources Reports , FAO, Rome., 2001.

Duzgoren-Aydin, N. S. and Aydin, A.: Chemical heterogeneities of weathered IgneousProfiles: implications for chemical indices, Environ. Eng. Geosci., 9(4), 363–376, 2003.

720 Dynarski, K. A., Morford, S. L., Mitchell, S. A. and Houlton, B. Z.: Bedrock nitrogen weathering stimulates biological nitrogen fixation, Ecology, 100(8), 1–10, doi:10.1002/ecy.2741, 2019.

Eggleton, R. A., Foudoulis, C. and Varkevisser, D.: Weathering of basalt: changes in rock chemistry and mineralogy, Clays Clay Miner., 35(3), 161–169, 1987.

EMBRAPA: Documentos 132 Manual de Métodos de, Embrapa, (ISSN 1517-2627), 230, 2011.

725 EMBRAPA: Manual de metodos de analises., 2017.

Ferreira, R. G., da Silva, D. D., Elesbon, A. A. A., Fernandes-Filho, E. I., Veloso, G. V., de Souza Fraga, M. and Ferreira, L. B.: Machine learning models for streamflow regionalization in a tropical watershed, J. Environ. Manage., 280, 111713, 2021.

Fioriob, P. R.: Estimation of Soil Properties by Orbital and Laboratory Reflectance Means and its Relation with Soil 730 Classification, Open Remote Sens. J., 2(1), 12–23, doi:10.2174/187541390100201012, 2013.

Fongaro, C. T., Demattê, J. A. M., Rizzo, R., Safanelli, J. L., Mendes, W. de S., Dotto, A. C., Vicente, L. E., Franceschini, M. H. D. and Ustin, S. L.: Improvement of clay and sand quantification based on a novel approach with a focus on multispectral satellite images, Remote Sens., 10(10), doi:10.3390/rs10101555, 2018.

Friedman, S. P.: Soil properties influencing apparent electrical conductivity : a review, , 46, 45–70, 735 doi:10.1016/j.compag.2004.11.001, 2005.

Fritsch, E. and Fitzpatrick, R. W.: Interpretation of soil features produced by ancient and modern processes in degraded landscapes. 1. A new method for constructing conceptual soil-water-landscape models, Soil Res., 32(5), 889–907, 1994.

Fritz, R. M., Malo, D. D., Schumacher, T. E., Clay, D. E., Carlson, C. G., Ellsbury, M. M. and Dalsted, K. J.: Field comparison of two soil electrical conductivity measurement systems, in Proceedings of the fourth international conference 740 on precision agriculture, pp. 1211–1217, Wiley Online Library., 1999.

Gaillardet, J., Dupre, B., Louvat, P. and Allegre, C. J.: Global silicate weathering and CO2 consumption rates deduced from the chemistry of large rivers, Chem. Geol., 159, 3–30, doi:10.1016/S0009-2541(99)00031-5, 1999.

Geonics, E. M.: EM38 Ground Conductivity Meter Operating Manual, Geonics Ltd. Ontario Mississauga, ON, Canada, 32, 2002.

745 Goddéris, Y., Roelandt, C., Schott, J., Pierret, M. C. and François, L. M.: Towards an integrated model of weathering, climate, and biospheric processes, Rev. Mineral. Geochemistry, 70, 411–434, doi:10.2138/rmg.2009.70.9, 2009.

Goh, K. M., Maulidiani, M., Rudiyanto, R., Abas, F., Lai, O. M., Nyam, K. L., Alharthi, F. A., Nehdi, I. A. and Tan, C. P.: The detection of glycidyl ester in edible palm-based cooking oil using FTIR-chemometrics and 1H NMR analysis, Food Control, 125, 108018, doi:https://doi.org/10.1016/j.foodcont.2021.108018, 2021.

750 Gomes, L. C., Faria, R. M., Souza, E. De, Veloso, G. V., Ernesto, C., Schaefer, G. R., Inácio, E. and Filho, F.: Modelling and mapping soil organic carbon stocks in Brazil, Geoderma, 340, 337–350, doi:10.1016/j.geoderma.2019.01.007, 2019.

Goydaragh, M. G., Taghizadeh-Mehrjardi, R., Golchin, A., Jafarzadeh, A. A. and Lado, M.: Predicting weathering indices in soils using FTIR spectra and random forest models, CATENA, 204, 105437, 2021.

Grasty, R. L., Holman, P. B. and Blanchard, Y. B.: Transportable calibration pads for ground and airborne gamma-ray spectrometers, Geological Survey of Canada., 1991.

Grimley, D. A. and Vepraskas, M. J.: Magnetic Susceptibility for Use in Delineating Hydric Soils, Soil Sci. Soc. Am. J., 64(6), 2174–2180, doi:10.2136/sssaj2000.6462174x, 2000.

Grimley, D. A., Arruda, N. K. and Bramstedt, M. W.: Using magnetic susceptibility to facilitate more rapid, reproducible and precise delineation of hydric soils in the midwestern USA, Catena, 58(2), 183–213, doi:10.1016/j.catena.2004.03.001, 2004.

Grubbs, R. A., Straw, C. M., Bowling, W. J., Radcliffe, D. E., Taylor, Z. and Henry, G. M.: Predicting spatial structure of soil physical and chemical properties of golf course fairways using an apparent electrical conductivity sensor, Precis. Agric., 20(3), 496–519, doi:10.1007/s11119-018-9593-2, 2019.

Harnois, L.: The CIW index: a new chemical index of weathering, Sediment. Geol., 55(3), 319–322, 1988.

Hasri, N. N. M., Wen, N. H., Howe, C. W., Mohamad, M. S., Deris, S. and Kasim, S.: Improved support vector machine using multiple SVM-RFE for cancer classification, Int. J. Adv. Sci. Eng. Inf. Technol., 7(4–2), 1589–1594, 2017.

Heil, K. and Schmidhalter, U.: Theory and Guidelines for the Application of the Geophysical Sensor EM38, , 38, 2019.

Hendrickx, ; Kachanoski, R. .: Miscible Solute Transport -Solute Content and Concentration - Indirect Measurement of Solute Concentration: Electromagnetic Induction, in Methods of Soil Analysis, vol. Chapter 6., 2002.

Hepper, E. N., Buschiazzo, D. E., Hevia, G. G., Urioste, A. and Antón, L.: Clay mineralogy, cation exchange capacity and specific surface area of loess soils with different volcanic ash contents, Geoderma, 135, 216–223, 2006.

Hijmans, R. J. and Van Etten, J.: raster: Geographic Data Analysis and Modeling. R package version 2.5-8, 2016.

Honeyborne, I., McHugh, T. D., Kuittinen, I., Cichonska, A., Evangelopoulos, D., Ronacher, K., van Helden, P. D., Gillespie, S. H., Fernandez-Reyes, D., Walzl, G., Rousu, J., Butcher, P. D. and Waddell, S. J.: Profiling persistent tubercule bacilli from patient sputa during therapy predicts early drug efficacy, BMC Med., 14(1), 1–13, doi:10.1186/s12916-016-0609-3, 2016.

IUSS Working Group WRB: World reference base for soil resources 2014. International soil classification system for naming soils and creating legends for soil maps., 2015.

J. A. Quaggio, Raij, B.: Determination of pH in calcium chloride and total acidity., Chem. Anal. Fertil. Eval. Trop. Soils. Inst. Agronômico Campinas, Campinas, 181–188, 2001.

Jackson, M. L.: Frequency distribution of clay minerals in major great soil groups as related to the factors of soil formation, Clays Clay Miner., 6(1), 133–143, 1957.

Jackson, M. L. and Sherman, G. D.: Chemical Weathering of Minerals in Soils, Adv. Agron., 5(C), 219–318, doi:10.1016/S0065-2113(08)60231-X, 1953.

Jambu, M.: Exploratory and multivariate data analysis, Elsevier., 1991.

Jayawardena, U. de S. and Izawa, E.: A new chemical index of weathering for metamorphic silicate rocks in tropical regions: A study from Sri Lanka, Eng. Geol., 36(3–4), 303–310, 1994.

Jenny, H.: Factors of soil formation: A system of quantitative pedology, Dover publication, New York., 1994.

790 Jiménez, C., Benavides, J., Ospina-Salazar, D. I., Zúñiga, O., Ochoa, O. and Mosquera, C.: Relationship between physical properties and the magnetic susceptibility in two soils of Valle del Cauca Relación entre propiedades físicas y la susceptibilidad magnética en dos suelos del Valle del Cauca, Cauca. Rev. Cienc. Agri, 34(341), 33–45, doi:10.22267/rcia.173402.70, 2017.

Johnston, M. A., Savage, M. J., Moolman, J. H. and du Plessis, H. M.: Evaluation of Calibration Methods for Interpreting Soil Salinity from Electromagnetic Induction Measurements, Soil Sci. Soc. Am. J., 61(6), 1627–1633,

795 doi:10.2136/sssaj1997.03615995006100060013x, 1997.

De Jong, E., Kozak, L. M. and Rostad, H. P. W.: Effects of parent material and climate on the magnetic susceptibility of Saskatchewan soils, Can. J. Soil Sci., 80(1), 135–142, doi:10.4141/s99-051, 2000.

Jung, Y., Lee, J., Lee, M., Kang, N. and Lee, I.: Probabilistic analytical target cascading using kernel density estimation for accurate uncertainty propagation, Struct. Multidiscip. Optim., 1–19, 2020.

800 Kassambara, A. and Mundt, F.: Package 'factoextra,' Extr. Vis. results Multivar. data Anal., 76, 2017.

Kaushal, S. S., Duan, S., Doody, T. R., Haq, S., Smith, R. M., Newcomer, T. A., Delaney, K., Gorman, J., Bowman, N., Mayer, P. M., Wood, K. L., Belt, K. T. and Stack, W. P.: Applied Geochemistry Human-accelerated weathering increases salinization , major ions , and alkalinization in fresh water across land use, Appl. Geochemistry, 83, 121–135, doi:10.1016/j.apgeochem.2017.02.006, 2017.

805 Ker, J. C., Curi, N., Schaefer, C. E. G. R. and Vidal-Torrado, P.: Pedologia: fundamentos, 2015.

Khelfaoui, M., Medjram, M. S., Kabir, A., Zouied, D., Mehri, K., Chikha, O. and Trabelsi, M. A.: Chemical and mineralogical characterization of weathering products in mine wastes, soil, and sediment from the abandoned Pb/Zn mine in Skikda, Algeria, Environ. Earth Sci., 79(12), 1–15, doi:10.1007/s12665-020-09043-x, 2020.

Kim, J. H., Jobbágy, E. G., Richter, D. D., Trumbore, S. E. and Jackson, R. B.: Agricultural acceleration of soil carbonate

810 weathering, Glob. Chang. Biol., 2020.

Kodikara, G. R. L. and McHenry, L. J.: Machine learning approaches for classifying lunar soils, Icarus, 345, 113719, 2020.

Kohavi, R. and John, G. H.: Wrappers for feature subset selection, Artif. Intell., 97(1–2), 273–324, 1997.

Kuhn, M. and Johnson, K.: Applied predictive modeling, Springer., 2013.

Kuhn, M., Wing, J., Weston, S., Williams, A., Keefer, C., Engelhardt, A., Cooper, T., Mayer, Z., Kenkel, B. and Team, R.

815 C.: Package 'caret,' R J., 2020.

Kumar, P., Kumar, N., Ambrish, M. and Mahajan, K.: Major ion chemistry , catchment weathering and water quality of Renuka Lake , north - west Himalaya , India, Environ. Earth Sci., 78(10), 1–16, doi:10.1007/s12665-019-8315-z, 2019.

Landis, J. R. and Koch, G. G.: The measurement of observer agreement for categorical data, Biometrics, 159–174, 1977.

Lerman, A., Wu, L. and Mackenzie, F. T.: CO2 and H2SO4 consumption in weathering and material transport to the ocean,

820 and their role in the global carbon balance, Mar. Chem., 106(1-2 SPEC. ISS.), 326–350, doi:10.1016/j.marchem.2006.04.004, 2007.

Lesch, S. M., Rhoades, J. D., Lund, L. J. and Corwin, D. L.: Mapping soil salinity using calibrated electromagnetic measurements, Soil Sci. Soc. Am. J., 56(2), 540–548, 1992.

Lim, C.H., Jackson, M. L.: Dissolution for total elemental analysis, in Methods of Soil Analysis. Part 2: Chemical and
825 Microbiological Properties., edited by Madison, pp. 1–12, American Society of Agronomy., 1986.

Linden, C. Vander and Delvaux, B.: Geoderma The weathering stage of tropical soils a ff ects the soil-plant cycle of silicon , but depending on land use, Geoderma, 351(May), 209–220, doi:10.1016/j.geoderma.2019.05.033, 2019.

Loughnan, F. C.: Some considerations in the weathering of the silicate minerals, J. Sediment. Res., 32(2), 284–290, 1962.

Maher, K.: The role of fluid residence time and topographic scales in determining chemical fluxes from landscapes, Earth
830 Planet. Sci. Lett., 312(1–2), 48–58, doi:10.1016/j.epsl.2011.09.040, 2011.

Marta, A., Castanheira, N., Farzamian, M., Catarina, M., Conceição, M., Monteiro, F. A. and Trianta, J.: Geoderma Prediction of soil salinity and sodicity using electromagnetic conductivity imaging, , 361(April 2019), doi:10.1016/j.geoderma.2019.114086, 2020.

Matsuura, D., Chounan, Y., Sugahara, Y. and Takeda, Y.: Wearable Working Assist Mechanism for Hemiplegics Capable of
835 Changing Step Length and Walking Direction, in New Trends in Medical and Service Robotics, pp. 126–133, Springer., 2019.

Maxbauer, D. P., Feinberg, J. M. and Fox, D. L.: Magnetic mineral assemblages in soils and paleosols as the basis for paleoprecipitation proxies: A review of magnetic methods and challenges, Earth-Science Rev., 155, 28–48, doi:10.1016/j.earscirev.2016.01.014, 2016.

840 McBratney, A. B., Mendonça Santos, M. L. and Minasny, B.: On digital soil mapping., 2003.

McFadden, M. and Scott, W. R.: Broadband soil susceptibility measurements for EMI applications, J. Appl. Geophys., 90, 119–125, doi:10.1016/j.jappgeo.2013.01.009, 2013.

Mcneill, J. D.: Rapid, accurate mapping of soil salinity by electromagnetic ground conductivity meters, , (30), 2–3, 1992.

McNeill, J. D.: Geonics EM38 ground conductivity meter, Tech. Note TN-21. Geonics Ltd., Mississauga, Ontario, Canada,
845 1986.

Mello, D., Demattê, J. A. M., Silvero, N. E. Q., Di Raimo, L. A. D. L., Poppiel, R. R., Mello, F. A. O., Souza, A. B., Safanelli, J. L., Resende, M. E. B. and Rizzo, R.: Soil magnetic susceptibility and its relationship with naturally occurring processes and soil attributes in pedosphere, in a tropical environment, Geoderma, 372(March), 114364, doi:10.1016/j.geoderma.2020.114364, 2020.

850 Mello, D., Alexandre Melo Demattê, J., Alcantara de Oliveira Mello, F., Roberto Poppiel, R., ElizabetQuiñonez Silvero, N., Lucas Safanelli, J., Barros e Souza, A., Augusto Di Loreto Di Raimo, L., Rizzo, R., Eduarda Bispo Resende, M. and Ernesto Gonçalves Reynaud Schaefer, C.: Applied gamma-ray spectrometry for evaluating tropical soil processes and attributes, Geoderma, 381, doi:10.1016/j.geoderma.2020.114736, 2021.

Migoń, P.: Weathering and hillslope development, John F. Schroder (ed.), Treatise Geomorphol., Vol. 4(San Diego:
855 Academic Press), 159–178., 2013a.

Migoń, P.: Weathering mantles and long-term landform evolution, John F. Schroder (ed.), Treatise Geomorphol., 4(San Diego: Academic Press), 127–144., 2013b.

Minty, B. R. S.: A Review of Airborne Gamma-Ray Spectrometric Data-Processing Techniques, Aust. Gov. Publ. Serv., 1988.

860 Modenesi, M. C.: Weathering and morphogenesis in a tropical plateau, Catena, 10(1–2), 237–251, 1983.

Nanni, M. R. and Demattê, J. A. M.: Spectral Reflectance Methodology in Comparison to Traditional Soil Analysis, Soil Sci. Soc. Am. J., 70(2), 393–407, doi:10.2136/sssaj2003.0285, 2006.

Navarre-Sitchler, A. and Brantley, S.: Basalt weathering across scales, Earth Planet. Sci. Lett., 261(1–2), 321–334, doi:10.1016/j.epsl.2007.07.010, 2007.

865 Neogi, S. and Dauwels, J.: Factored Latent-Dynamic Conditional Random Fields for Single and Multi-label Sequence Modeling, arXiv Prepr. arXiv1911.03667, 2019.

Nocco, M. A., Ruark, M. D. and Kucharik, C. J.: Geoderma Apparent electrical conductivity predicts physical properties of coarse soils, Geoderma, 335(July 2018), 1–11, doi:10.1016/j.geoderma.2018.07.047, 2019.

Nordt, L. C. and Driese, S. D.: New weathering index improves paleorainfall estimates from Vertisols, Geology, 38(5), 407–
870 410, 2010.

Ollier, C.: Weathering, edited by Second edition, Longman., 1984.

Osher, L. J. and Buol, S. W.: Relationship of soil properties to parent material and landscape position in eastern Madre de Dios, Peru, Geoderma, 83(1–2), 143–166, 1998.

Pansu, M., Gautheyrou, J.: Handbook of Soil Analysis – Mineralogical, Organic and Inorganic Methods., Springer,
875 Netherlands., 2006.

Peralta, N. R., Costa, J. L., Balzarini, M. and Angelini, H.: Delineation of management zones with measurements of soil apparent electrical conductivity in the southeastern pampas, Can. J. Soil Sci., 93(2), 205–218, 2013.

Porder, S.: How Plants Enhance Weathering and How Weathering is Important to Plants, Elements, 15(4), 241–246, doi:10.2138/gselements.15.4.241, 2019.

880 Pozdnyakov, A. I.: Electrical parameters of soils and pedogenesis, Eurasian Soil Sci., 41(10), 1050–1058, doi:10.1134/S1064229308100062, 2008.

Prasetyo, B. H., Suharta, N., H., S. and Hikmatullah, H.: Chemical and Mineralogical Properties of Ultisols of Sasamba Area, East Kalimantan, Indones. J. Agric. Sci., 2(2), 37, doi:10.21082/ijas.v2n2.2001.p37-47, 2016.

R Core Team: R: A Language and Environment for Statistical Computing, R Foundation for Statistical Computing, Vienna,
885 Austria., 2015.

Regmi, Amar; Yoshida, Kohki; Dhital, Megh; Pradhan, B.: Weathering and mineralogical variation in gneissic rocks and their effect in Sangrumba Landslide , East Nepal, , 2711–2727, doi:10.1007/s12665-013-2649-8, 2014.

Reinhardt, N. and Herrmann, L.: Gamma-ray spectrometry as versatile tool in soil science: A critical review, J. Plant Nutr. Soil Sci., 182(1), 9–27, doi:10.1002/jpln.201700447, 2019.

890   Rhoades, J. D., Corwin, D. L. and Lesch, S. M.: Geospatial measurements of soil electrical conductivity to assess soil salinity and diffuse salt loading from irrigation, Geophys. Monogr. Geophys. Union, 108, 197–216, 1999a.

Rhoades, J. D., Chanduvi, F. and Lesch, S. M.: Soil salinity assessment: Methods and interpretation of electrical conductivity measurements, Food & Agriculture Org., 1999b.

Ribeiro, F. C. A., Silva, J. I. R., Lima, E. S. A., do Amaral Sobrinho, N. M. B., Perez, D. V. and Lauria, D. C.: Natural

895   radioactivity in soils of the state of Rio de Janeiro (Brazil): Radiological characterization and relationships to geological formation, soil types and soil properties, J. Environ. Radioact., 182(November 2017), 34–43, doi:10.1016/j.jenvrad.2017.11.017, 2018.

Richards, L. A.: Diagnosis and improvement of saline and alkali soils, LWW., 1954.

Rochette, P., Jackson, M. and Aubourg, C.: Rock magnetism andn the interpretation of magnetic susceptibility, Rev.

900   Geophys., 30(3), 209–226, 1992.

Ruxton, B. P.: Measures of the degree of chemical weathering of rocks, J. Geol., 76(5), 518–527, 1968.

Rytky, S. J. O., Tiulpin, A., Frondelius, T., Finnilä, M. A. J., Karhula, S. S., Leino, J., Pritzker, K. P. H., Valkealahti, M., Lehenkari, P., Joukainen, A., Kröger, H., Nieminen, H. J. and Saarakkala, S.: Automating three-dimensional osteoarthritis histopathological grading of human osteochondral tissue using machine learning on contrast-enhanced micro-computed

905   tomography, Osteoarthr. Cartil., 28(8), 1133–1144, doi:10.1016/j.joca.2020.05.002, 2020.

Saidian, M., Godinez, L. J. and Prasad, M.: Effect of clay and organic matter on nitrogen adsorption specific surface area and cation exchange capacity in shales (mudrocks), in SPWLA 56th Annual Logging Symposium, OnePetro., 2015.

Samotoin, N. D. and Bortnikov, N. S.: Formation of kaolinite nano-and microcrystals by weathering of phyllosilicates, Geol. Ore Depos., 53(4), 340–352, 2011.

910   Santos-Francés, F., Gil Pacheco, E., Martínez-Graña, A., Alonso Rojo, P., Ávila Zarza, C. and García Sánchez, A.: Concentration of uranium in the soils of the west of Spain, Environ. Pollut., 236, 1–11, doi:10.1016/j.envpol.2018.01.038, 2018.

Santos, A. do C., Cipriano da Silva, R., Carvalho da Silva Neto, E., Cunha dos Anjos, L. H. and Pereira, M. G.: Weathering and pedogenesis of mafic rock in the Brazilian Atlantic Forest, J. South Am. Earth Sci., 111, 103452,

915   doi:https://doi.org/10.1016/j.jsames.2021.103452, 2021.

Dos Santos, H. G., Jacomine, P. K. T., Dos Anjos, L. H. C., De Oliveira, V. Á., Lumbreras, J. F., Coelho, M. R., De Almeida, J. A., de Araujo Filho, J. C., De Oliveira, J. B. and Cunha, T. J. F.: Brazilian Soil Classification System., Embrapa Solos-Livro técnico (INFOTECA-E), 2018.

Santos, J., Le, E., Souza, C., Oliveira, D., Severino, V., Júnior, D. S., Araújo, F. De, Metri, M., Carlos, A. and Azevedo, D.:

920   Geoderma Impact of weathering on REE distribution in soil-saprolite pro fi les developed on orthogneisses in Borborema Province , NE Brazil, Geoderma, 347(March), 103–117, doi:10.1016/j.geoderma.2019.03.040, 2019.

Sarmast, M., Farpoor, M. H. and Esfandiarpour Boroujeni, I.: Magnetic susceptibility of soils along a lithotoposequence in southeast Iran, Catena, 156(March), 252–262, doi:10.1016/j.catena.2017.04.019, 2017.

Scarciglia, F., Le Pera, E., Vecchio, G. and Critelli, S.: The interplay of geomorphic processes and soil development in an
925   upland environment, Calabria, South Italy, Geomorphology, 69(1–4), 169–190, doi:10.1016/j.geomorph.2005.01.003, 2005.

Scarciglia, F., Critelli, S., Borrelli, L., Coniglio, S., Muto, F. and Perri, F.: Weathering pro fi les in granitoid rocks of the Sila
Massif uplands , Calabria , southern Italy : New insights into their formation processes and rates, Sediment. Geol., 336, 46–
67, doi:10.1016/j.sedgeo.2016.01.015, 2016.

Schaetzl, J Randall and Anderson, S.: Soil Genesis and Geomorphology, Cambridge University Press, New York., 2005.

930   Schaetzl, R. and Anderson, S.: Soils. Genesis and Geomorphology, Cambridge University Press, New York., 2005.

Schuessler, J. A., von Blanckenburg, F., Bouchez, J., Uhlig, D. and Hewawasam, T.: Nutrient cycling in a tropical montane
rainforest under a supply-limited weathering regime traced by elemental mass balances and Mg stable isotopes, Chem. Geol.,
497(July), 74–87, doi:10.1016/j.chemgeo.2018.08.024, 2018.

Schuler, U., Erbe, P., Zarei, M., Rangubpit, W., Surinkum, A., Stahr, K. and Herrmann, L.: A gamma-ray spectrometry
935   approach to field separation of illuviation-type WRB reference soil groups in northern Thailand, J. Plant Nutr. Soil Sci.,
174(4), 536–544, doi:10.1002/jpln.200800323, 2011.

Schwertmann, U.: Occurrence and formation of iron oxides in various pedoenvironments, Iron soils clay Miner., 267–308,
doi:10.1007/978-94-009-4007-9_11, 1988.

Scott, A. J. and Symons, M. J.: Clustering methods based on likelihood ratio criteria, Biometrics, 387–397, 1971.

940   Seasholtz, M. B. and Kowalski, B.: The parsimony principle applied to multivariate calibration, Anal. Chim. Acta, 277(2),
165–177, 1993.

Setiawan, O., Sartohadi, J., Hadi, M. P. and Mardiatno, D.: Infiltration characterization using principal component analysis
and K-means cluster analysis on quaternary volcanic landscape at the southern flank of Rinjani Volcano, Lombok Island,
Indonesia, Phys. Geogr., 41(3), 217–237, 2020.

945   Shenggao, L.: Lithological factors affecting magnetic susceptibility of subtropical soils, Zhejiang Province, China, Catena,
40(4), 359–373, doi:10.1016/S0341-8162(00)00092-8, 2000.

Silva, C. S., Silva-Filho, F. C., Santos, A. D., COSCIONE, A. R., Vitti, A., BOARETTO, A., Coelho, J. A. P., Bvan, R.,
Silva, C. A. and Abreu, C. H.: Manual de análises químicas de solos, plantas e fertilizantes., 2009.

Silvero, N. E. Q., Demattê, J. A. M., de Souza Vieira, J., de Oliveira Mello, F. A., Amorim, M. T. A., Poppiel, R. R., de
950   Sousa Mendes, W. and Bonfatti, B. R.: Soil property maps with satellite images at multiple scales and its impact on
management and classification, Geoderma, 397, 115089, 2021.

Solutions, R.: Spectrum stabilization and calibration for the RSI RS-125 and RS-230 handheld spectrometers, 2009.

Son, Y., Oh, M. and Lee, S.: Estimation of soil weathering degree using electrical resistivity, Environ. Earth Sci., 59(6),
1319–1326, doi:10.1007/s12665-009-0119-0, 2010.

955   Sudduth, K. A., Drummond, S. T. and Kitchen, N. R.: Accuracy issues in electromagnetic induction sensing of soil electrical
conductivity for precision agriculture, Comput. Electron. Agric., 31(3), 239–264, 2001.

Sudduth, K. A., Kitchen, N. R., Wiebold, W. J., Batchelor, W. D., Bollero, G. A., Bullock, D. G., Clay, D. E., Palm, H. L., Pierce, F. J., Schuler, R. T. and Thelen, K. D.: Relating apparent electrical conductivity to soil properties across the north-central USA, , 46, 263–283, doi:10.1016/j.compag.2004.11.010, 2005.

960   Syed, H. S.: Comparison studies adsorption of thorium and uranium on pure clay minerals and local Malaysian soil sediments, J. Radioanal. Nucl. Chem., 241(1), 11–14, doi:10.1007/BF02347283, 1999.

Taylor, J. A., Coulouma, G., Lagacherie, P. and Tisseyre, B.: Mapping soil units within a vineyard using statistics associated with high-resolution apparent soil electrical conductivity data and factorial discriminant analysis, Geoderma, 153(1–2), 278–284, 2009.

965   Taylor, M. J., Smettem, K., Pracilio, G. and Verboom, W.: Relationships between soil properties and high-resolution radiometrics, central eastern Wheatbelt, Western Australia, Explor. Geophys., 33(2), 95–102 [online] Available from: https://doi.org/10.1071/EG02095, 2002.

Terra, F. S., Demattê, J. A. M. and Viscarra Rossel, R. A.: Proximal spectral sensing in pedological assessments: vis–NIR spectra for soil classification based on weathering and pedogenesis, Geoderma, 318(October 2017), 123–136,
970   doi:10.1016/j.geoderma.2017.10.053, 2018.

Torres, M. A., West, A. J., Clark, K. E., Paris, G., Bouchez, J., Ponton, C., Feakins, S. J., Galy, V. and Adkins, J. F.: The acid and alkalinity budgets of weathering in the Andes–Amazon system: Insights into the erosional control of global biogeochemical cycles, Earth Planet. Sci. Lett., 450, 381–391, doi:10.1016/j.epsl.2016.06.012, 2016.

Tsering, T., Abdel, M. S. M., Iftekhar, S. and Sillanpää, M.: Journal of Hydrology : Regional Studies Major ion chemistry of
975   the Teesta River in Sikkim Himalaya , India : Chemical weathering and assessment of water quality, J. Hydrol. Reg. Stud., 24(January), 100612, doi:10.1016/j.ejrh.2019.100612, 2019.

Turkington, A. V., Phillips, J. D. and Campbell, S. W.: Weathering and landscape evolution, Geomorphology, 67(1-2 SPEC. ISS.), 1–6, doi:10.1016/j.geomorph.2004.08.013, 2005.

Valaee, M., Ayoubi, S., Khormali, F., Lu, S. G. and Karimzadeh, H. R.: Using magnetic susceptibility to discriminate
980   between soil moisture regimes in selected loess and loess-like soils in northern Iran, J. Appl. Geophys., 127, 23–30, doi:10.1016/j.jappgeo.2016.02.006, 2016.

Vandenhove, H., Van Hees, M., Wouters, K. and Wannijn, J.: Can we predict uranium bioavailability based on soil parameters? Part 1: Effect of soil parameters on soil solution uranium concentration, Environ. Pollut., 145(2), 587–595, doi:10.1016/j.envpol.2006.04.011, 2007.

985   Varga-Szemes, A., Schoepf, U. J., Maurovich-Horvat, P., Wang, R., Xu, L., Dargis, D. M., Emrich, T. and Buckler, A. J.: Coronary plaque assessment of Vasodilative capacity by CT angiography effectively estimates fractional flow reserve, Int. J. Cardiol., 331, 307–315, doi:https://doi.org/10.1016/j.ijcard.2021.01.040, 2021.

Viscarra Rossel, R. A., Webster, R. and Kidd, D.: Mapping gamma radiation and its uncertainty from weathering products in a Tasmanian landscape with a proximal sensor and random forest kriging, Earth Surf. Process. Landforms, 39(6), 735–748,
990   doi:10.1002/esp.3476, 2014.

Wang, L., Dai, L., Li, L. and Liang, T.: Multivariable cokriging prediction and source analysis of potentially toxic elements (Cr, Cu, Cd, Pb, and Zn) in surface sediments from Dongting Lake, China, Ecol. Indic., 94, 312–319, 2018.

Wang, Y.-B., Liu, C.-W. and Wang, S.-W.: Characterization of heavy-metal-contaminated sediment by using unsupervised multivariate techniques and health risk assessment, Ecotoxicol. Environ. Saf., 113, 469–476, 2015.

995 White, W. M.: Encyclopedia of Geochemistry: A Comprehensive Reference Source on the Chemistry of the Earth, Springer International Publishing., 2018.

Wilford, J.: A weathering intensity index for the Australian continent using airborne gamma-ray spectrometry and digital terrain analysis, Geoderma, 183–184, 124–142, doi:10.1016/j.geoderma.2010.12.022, 2012.

Wilford, J. and Minty, B.: Chapter 16 The Use of Airborne Gamma-ray Imagery for Mapping Soils and Understanding

1000 Landscape Processes, Dev. Soil Sci., 31(C), doi:10.1016/S0166-2481(06)31016-1, 2006.

Wilford, P. N., Bierwirth, J. R. and Craig, M. A.: Application of airborne gamma-ray spectrometry in soiVregolith mapping and Applied Geomorphology, , 17(2), 1997.

Yoo, K., Mudd, S. M., Sanderman, J., Amundson, R. and Blum, A.: Spatial patterns and controls of soil chemical weathering rates along a transient hillslope, Earth Planet. Sci. Lett., 288(1–2), 184–193, doi:10.1016/j.epsl.2009.09.021, 2009.

1005 Young, G. M. and Nesbitt, H. W.: Processes controlling the distribution of Ti and Al in weathering profiles, siliciclastic sediments and sedimentary rocks, J. Sediment. Res., 68(3), 448–455, 1998.

Yu, C., Peng, B., Peltola, P., Tang, X. and Xie, S.: Effect of weathering on abundance and release of potentially toxic elements in soils developed on Lower Cambrian black shales, P. R. China, Environ. Geochem. Health, 34(3), 375–390, doi:10.1007/s10653-011-9398-y, 2012.

1010 Zhang, Y. and Hartemink, A. E.: Data fusion of vis – NIR and PXRF spectra to predict soil physical and chemical properties, Eur. J. Soil Sci., (May 2019), 316–333, doi:10.1111/ejss.12875, 2020.

Zhu, F., Xue, S. and Hartley, W.: Novel predictors of soil genesis following natural weathering processes of bauxite residues, , 2856–2863, doi:10.1007/s11356-015-5537-9, 2016.

Zuber, S. M., Behnke, G. D., Nafziger, E. D. and Villamil, M. B.: Multivariate assessment of soil quality indicators for crop

1015 rotation and tillage in Illinois, Soil Tillage Res., 174, 147–155, 2017.